Medical Image Analysis 72 (2021) 102082

Contents lists available at ScienceDirect

Medical Image Analysis

journal homepage: www.elsevier.com/locate/media

Deep Fusion of Brain Structure-Function in Mild Cognitive Impairment

Lu Zhang[a], Li Wang[a,b], Jean Gao[a], Shannon L. Risacher[c], Jingwen Yan[d], Gang Li[e], Tianming Liu[f], Dajiang Zhu[a,*], for the Alzheimer's Disease Neuroimaging Initiative[1]

[a] Department of Computer Science and Engineering, The University of Texas at Arlington, Arlington, TX 76019 USA
[b] Department of Mathematics, The University of Texas at Arlington, Arlington, TX 76019 USA
[c] Department of Radiology and Imaging Sciences, Indiana University School of Medicine, Indianapolis, IN 46202 USA
[d] School of Informatics and Computing, Indiana University School of Medicine, Indianapolis, IN 46202 USA
[e] Biomedical Research Imaging Center and Department of Radiology, University of North Carolina at Chapel Hill, Chapel Hill, NC 27599-7160, USA
[f] Cortical Architecture Imaging and Discovery Lab, Department of Computer Science and Bioimaging Research Center, The University of Georgia, Athens, GA, USA

ARTICLE INFO

Article history:
Received 12 November 2020
Revised 20 March 2021
Accepted 13 April 2021
Available online 23 April 2021

Keywords:
Brain structure and function fusion
graph-based deep learning
MCI

ABSTRACT

Multimodal fusion of different types of neural image data provides an irreplaceable opportunity to take advantages of complementary cross-modal information that may only partially be contained in single modality. To jointly analyze multimodal data, deep neural networks can be especially useful because many studies have suggested that deep learning strategy is very efficient to reveal complex and non-linear relations buried in the data. However, most deep models, e.g., convolutional neural network and its numerous extensions, can only operate on regular Euclidean data like voxels in 3D MRI. The inter-related and hidden structures that beyond the grid neighbors, such as brain connectivity, may be over-looked. Moreover, how to effectively incorporate neuroscience knowledge into multimodal data fusion with a single deep framework is understudied. In this work, we developed a graph-based deep neural network to simultaneously model brain structure and function in Mild Cognitive Impairment (MCI): the topology of the graph is initialized using structural network (from diffusion MRI) and iteratively updated by incorporating functional information (from functional MRI) to maximize the capability of differentiating MCI patients from elderly normal controls. This resulted in a new connectome by exploring "deep relations" between brain structure and function in MCI patients and we named it as Deep Brain Connectome. Though deep brain connectome is learned individually, it shows consistent patterns of alteration comparing to structural network at group level. With deep brain connectome, our developed deep model can achieve 92.7% classification accuracy on ADNI dataset.

Introduction

With the availability of large-scale multiple types of brain image data, integration of data acquired from different imaging techniques, termed as multimodal data fusion (Damoiseaux & Greicius (2009); Wee et al. (2012); Park & Friston (2013); Sui et al. (2012, 2014); Suk et al. (2014); Uludağ & Roebroeck (2014); Zhu et al. (2014b)), has gained considerable attention in neuroimaging field. Multimodal fusion provides an irreplaceable opportunity to take advantages of complementary cross-modal information that may only partially be contained in single modality data. Essentially, each imaging modality provides a different but unique view to represent brain structure and/or function. For example, diffusion tensor imaging (DTI) can provide information of brain structural connectivity (e.g., via tractography (Mori et al. (1999)), and blood oxygen level-dependent (BOLD) signals derived from functional magnetic resonance imaging (fMRI) can be used to infer neural activity in vivo through measuring hemodynamic response. By jointly analyzing DTI and fMRI data we can investigate organizational architecture of human brain in both structural and functional domains. Besides studying general relationships between brain structure and function, multimodal data fusion can provide complementary knowledge when exploring and identifying potential abnormalities occurred in brain disorders. Mild cognitive impairment (MCI) is considered the precursor of Alzheimer's disease, which is a progressive and irreversible neurodegenerative disorder characterized by severe cognitive decline and memory loss. Though the neuropathological mechanism

* Corresponding author at: Dajiang Zhu, 500 UTA Blvd., Room 640, Box 19015, Arlington TX 76019.
E-mail address: dajiang.zhu@uta.edu (D. Zhu).

[1] Data used in preparation of this article were obtained from the Alzheimer's Disease Neuroimaging Initiative (ADNI) database. (adni.loni.usc.edu).

https://doi.org/10.1016/j.media.2021.102082
1361-8415/

is not fully understood, increasing evidences have shown that both structural and functional brain alterations are found in MCI patients (Supekar et al. (2008); Xie & He (2012); Chen et al. (2013); Daianu et al. (2013); Franzmeier & Dyrba (2017); Dai et al. (2019)). As a result, using single modality, e.g., either structural or functional data, for brain disease studies including classification or prediction, can be suboptimal.

Many multimodal fusion approaches have been published for cognitive and clinical studies (Schonberg et al. (2006); Honey et al. (2009); Hagmann et al. (2010); Fling et al. (2012); Jie et al. (2013); Suk et al. (2014); Meng et al. (2017); Liu et al. (2018); Zhang et al. (2019)) and more details will be reviewed in Section 2.1. Most multimodal data fusion approaches have been focusing on simple and linear relationship between different modalities (Plis et al. (2018)), while many studies have demonstrated the complexity between the information conveyed by different types of data: brain structure and function are closely related, but neither of them can fully interpret the organizational principles of human brain. Previous publications (Honey et al. (2009); Li et al. (2012)) suggested that strong structural connectivity inclines to be accompanied with strong functional connectivity, but not vice versa. The changes of brain structure or function may also result in the alterations of the other. For example, when a structural connection between two brain regions is reduced, these regions can increase neuronal activity to compensate for the loss of communications (Daselaar et al. (2015)).

As an emerging research topic, deep neural network based machine learning methods (Hinton & Salakhutdinov (2006)) can be especially useful in capturing the complex and non-linear relationship between brain structure and function in multimodal fusion. Recent development of deep learning has revolutionized the fields of artificial intelligence and machine learning (LeCun et al. (2015)), and boosted several domains such as computer vision (He et al. (2016)) and many others (Monti et al. (2017); Ying et al. (2018)). As one of the most popular deep models, convolutional neural network (LeCun et al. (1990)) (CNN) has demonstrated breakthroughs of performance in neuroimaging analysis including detection (Sirinukunwattana et al. (2016)), reconstruction (Sun et al. (2019)), segmentation (Wang et al. (2015)) and computer-aided diagnosis (Roth et al. (2015)). However, it could be difficult to directly apply CNN on brain network analysis, as CNN and its numerous extensions are designed for operations on regular, Euclidean data, such as pixels in 2D slices or voxels in 3D volumetric data. Whereas human brain is a highly complex and interconnected network that can efficiently coordinate regional segregation and specialization (Tononi et al. (1994); Bullmore & Sporns (2009); Fornito et al. (2015)). The connectivity, which indicates the influences from remote brain areas that have either structural connections or functional interactions, provides the physiological basis of information representation and processing in brain (Sporns et al. (2004); Fries (2005); Petersen & Sporns (2015); Lynn & Bassett (2019)). Therefore, the interrelated and hidden structures (i.e. modularity (Bullmore & Sporns (2009)) that beyond regular grid neighbors can be overlooked in traditional CNN approaches. In addition, most current deep neural network methods only focused on single modality data, such as structural, diffusion or functional MRI, very few studies have examined the multimodal data fusion using deep learning at network level. Though some deep models based on multimodal data have been proposed, the number and scope of studies are still very limited, and further efforts are highly needed to investigate appropriate strategies for exploring potential "deep relationship" between brain structure and function, as well as to develop disorder-focused deep modeling architecture.

Motivated by the merits of multimodal fusion in neuroimage studies and the recent advancement of graph convolutional network – GCN (Kipf & Welling (2016);Wu et al. (2020); Zhang et al. (2020b)), we leverage both by integrating them into a novel graph-based deep model (GBDM) to study brain structure-function fusion at connectome level. We construct a multi-layer GCN with trainable graph topology. This graph is parameterized by both DTI-derived brain structural network and functional activities so that the learned graph becomes a deeply hybrid connectome by retaining brain structural substrate and simultaneously taking into account the functional influences as a complementary cross-modal information. In general, our GBDM aims to maximize the performance of classifying MCI patients from elder normal controls by incorporating functional interactions into structural network. Fig. 1 illustrates the overall strategy of GBDM. During the training phase, we used structural network as the initialization of the graph (Fig. 1(b)). Functional information (Fig. 1(a)) is used in two ways: the fMRI BOLD signals of each pair of brain regions are parameterized to form trainable functional profiles which are integrated into the current graph at each iteration; the functional connectivity are treated as features associated with the nodes that represent different brain regions. GBDM iteratively updates the topology of the graph (Fig. 1(c)) to minimize its classification loss. In the prediction phase, given individual structural network and functional data, GBDM outputs the graph topology as well as the predicted clinical conditions. Because this predicted graph evolves from both structural and functional connectome in a deep manner, we named it as *Deep Brain Connectome*. Using ADNI (Alzheimer's Disease Neuroimaging Initiative) (http://adni.loni.usc.edu/) brain image dataset as a test bed, we generated deep brain connectome for each subject in both groups (MCI and aged normal controls). Compared to DTI derived structural connectome, the learned deep brain connectome displays decreased connectivity within the same hemisphere and increased connectivity across different hemispheres. These differences come from the integration of functional data when conducting classification task. Interestingly, the brain regions involved in the top changed connectivity are widely known for their close relations to AD/MCI development, such as lateral orbital and temporal regions. In addition, our experimental results show that the classification accuracy using our proposed GBDM yields up to 92.7%.

Our proposed deep multimodal fusion method advances the state of the art in three ways: first, a graph-based deep model is proposed to represent and manipulate brain connectome instead of using traditional CNN architecture which only considers the influences of Euclidean-based (local) neighbors. The primary motivation comes from the fact that one brain region might interact with other remote regions along the brain network topology. Many neurological symptoms are considered to be related to network level alternations rather than focal abnormality of brain (Zhu et al. (2014a), Vieira et al. (2017)). Second, the developed GBDM is trained based on structural network which is used to initialize the topology of the graph. The neurological rationality is that recent studies (Guo & Lee (2014); Phillips et al. (2019)) suggests that the neurodegenerative disease related pathogenic protein (e.g., Aβ and tau) may aggregate via long-distance transmission along white matter pathways between remote brain regions. Hence, it is natural to explore potential MCI/AD related abnormalities within individual structural network, instead of using Euclidean neighbors. Thirdly, most current deep learning methods focused on either brain structural or functional data, few studies have been conducted on both of them at network level. However, it is suggested that MCI/AD progression may follow both structural and functional topologies (Franzmeier & Dyrba (2017)). In our proposed GBDM, the topology of the graph is learned from functional features and structural network simultaneously, by maximizing MCI classification performance. The obtained deep brain con-

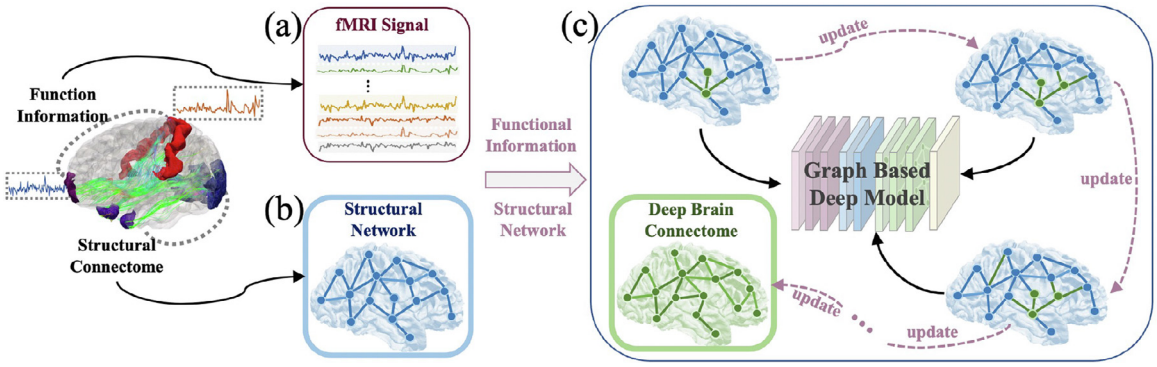

Fig. 1. Illustration of the proposed Deep Brian Connectome learning based on Graph Based Deep Model (GBDM). By using Destrieux atlas (Destrieux et al. (2010)) along with DTI and resting state fMRI data, we extracted the averaged BOLD signal of each brain region (148 regions in total) (Fig. 1(a)) and constructed brain structural network (Fig. 1(b)). Then the structural network was used as the initialization of graph topology, and the functional information was used by GBDM to iteratively update the topology of the graph – deep brain connectome (Fig. 1(c)), to maximize its classification power for MCI patients.

nectome reflects a deep fusion of structural and functional network alterations in MCI patients.

Related work

Multimodal Fusion

There are two widely used strategies to integrate potential complementary information buried in multimodal data for AD classification – feature concatenation and feature fusion. Feature concatenation is simply concatenating the features derived from different modalities and combining them as a single feature vector for classification. For example, many studies have tried to combine the features from structural MRI and other imaging modalities, such as diffusion MRI, functional MRI and positron emission tomography (PET), to improve the classification performance. Cui et al. (2012), Li et al. (2014), and Schouten et al. (2016) used the combination of regional volumetric measures extracted from structural MRI, diffusion measures generated from diffusion MRI and correlation measures calculated from functional MRI as input features to conduct AD classification. Tang et al. (2016) combined volumetric, shape and diffusion measures of hippocampus and amygdala into a high dimension feature vector. Then they used PCA and Student's t-tests to reduce the feature size and fed the selected features into Support Vector Machine (SVM) for AD classification. Fan et al. (2008) merged regional volumetric measures with regional fluorodeoxyglucose PET intensity for MCI classification using linear SVM. In their work, feature selection methods have been applied to improve the classification performance. The combination of imaging modalities with non-imaging features including demographics, cognitive measures, and genetic data has also been explored. Vemuri et al. (2008) integrated gray matter (GM), white matter (WM), and CSF density maps with demographics (age, gender), cognitive measures, and genetic data (APOE genotype) for single kernel SVM-based classification. Zhang et al. (2014) applied PCA on GM density maps, demographics and cognitive measures for feature extraction. Then based on the selected features, they constructed a single kernel support vector machine decision tree (kSVM-DT) for AD classification. Moradi et al. (2015) combined GM density maps, demographics (age), and cognitive tests as features, and employed a semi-supervised learning method – low-density separation, for AD conversion prediction. The advantages of feature concatenation are straightforward and easy to realize. However, this strategy has a major limitation: it treats multimodal features equally and ignores the different natures and underlying importance of various features extracted from different modalities (Hinrichs et al. (2011); Liu et al. (2013)). Feature fusion tries to accommodate different information contained in multiple modalities by designing more sophisticated ways to combine multimodal features. Dyrba et al. (2015) used regional GM volumetric measures, diffusion measures (FA, MD, and mode of anisotropy), functional measures (the shortest weighted path-length) and network measures (weighted local clustering) as features and adopted multi-kernel SVM for AD classification. Different from conventional SVM, multi-kernel SVM allows using different types of kernels for multimodal data and provides a promising way to account for the different natures of features extracted from different modalities. Similarly, Zhang et al. (2011, 2012) applied multi-kernel learning to regional GM volume, regional average FDG-PET intensity, and CSF biomarkers to conduct AD and MCI classification. Besides using different kernels for classification, different modalities can be used to train classifiers separately. Dai et al. (2012) trained multiple LDA classifiers based on regional GM volumetric measures and functional measures (functional connectivity strength, homogeneity, and amplitude of low-frequency fluctuations). Then, they combined the output of the classifiers by weighted voting. In general, both feature concatenation and fusion aim to integrate the knowledge from multiple sources by considering their simple (e.g., linear) relations using shallow models, the complex brain structure-function interactions have been overlooked.

Graph Convolutional Network in Neuroimaging

Recent advancement of graph convolutional network (GCN) (Kipf & Welling (2016); Wu et al. (2020); Zhang et al. (2020)) extends the convolutional operations from regular, Euclidean data to non-Euclidean data and witnesses great success in brain disease prediction (Ktena et al. (2018); Parisot et al. (2018); Kazi et al. (2019); Zhang et al. (2019a); Song et al. (2021)). Based on the definition of the graph, existing neuroimaging studies using GCN can be divided into two categories – population-level graph and individual-level graph. In population-level graph, each node in the graph represents one subject's data and the edge represents the similarity between the two connecting individuals. For example, Parisot et al. (2018) represented the whole populations by a sparse graph. They used imaging features of each subject as nodes and encoded pairwise similarities between features as edge weights. Based on the constructed sparse graph, a GCN was trained in a semi-supervised manner to predict conversion to Alzheimer's disease. Kazi et al. (2019) adopted a similar graph structure, where each node represented an individual and was associated with a feature vector generated from imaging data. The similarities between the individuals were calculated via non-imaging data. Different from conventional models that used con-

stant filter size throughout all layers, Kazi et al. (2019) proposed an InceptionGCN to generate class separable output features by varying the filters' size across the GCN layers. To better characterize the relationship between nodes and improve the classification performance, Song et al. (2021) designed a similarity-aware adaptive calibrated GCN (SAC-GCN). The SAC-GCN used a calibration mechanism to fuse fMRI and DTI information into edges and pre-trained a GCN to calculate the similarity between each pair of subjects. However, population-level graph is limited in flexibility when the sample size grows and in capability when representing rich information of individuals. Individual-level methods construct individual graph for each subject. Each node in the graph represents a region of interest (ROI), e.g., a brain region defined in brain atlas, and the edge indicates the relationships (e.g., connectivity) between the two ROIs. Zhang et al. (2019b) constructed multiple graphs for each subject with respect to multi-modal brain networks. They trained different GCNs and concatenated features generated by each GCN to conduct classification of Parkinsons disease. Ktena et al. (2018) built a single graph for each subject using functional connectivity and proposed a siamese graph convolutional network (s-GCN) to learn a graph similarity metric. In their work, two GCNs are constructed with shared weights and followed by a fully-connect (FC) layer. During the training process, two graphs from the same and different clinical groups are fed into the two GCNs respectively and the FC layer outputs the similarity estimate. In general, most GCN studies fix the topology of the graph throughout the training process. As a result, they are designed to study the the relations among different brain regions (nodes) from either structural or functional perspectives, instead of the interactions between brain structure and function.

Methods

Method Overview

We proposed a graph-based deep model (GBDM) (Fig. 2) to analyze brain structure-function abnormalities in MCI patients by integrating both structural and functional data. Brain structural network is used to initialize the topology of the graph, i.e., the adjacency matrix in GCN. An individual functional profile is learned and combined with structural network iteratively. Pearson's correlation coefficients of averaged BOLD signals are treated as the features associated with the nodes of the graph. The entire model is designed to differentiate MCI from NC by seamlessly incorporating functional profile learning (*Section 3.2*) and brain structure-function fusion (*Section 3.3*). Specifically, our model is composed of four components: 1) learning of functional profile to parameterize pairwise functional relations between any two brain regions; 2) brain structure-function fusion for seeking to best combine both structural network and the learned functional profile as new topology of the graph; 3) brain network convolution conducted upon the updated graph topology; 4) MCI-NC classification with fully connected neural network.

Functional Profile Learning

There exist a few measurements to represent pairwise relationship between two BOLD signals derived from fMRI, such as mutual information (Hlinka et al. (2011)), covariance (Challis et al. (2015)), correlation (Zhu et al. (2014a)) and partial correlation (Smith et al. (2011)). In general, how to effectively represent the functional relationships among brain regions is still an open research area. In this work, we aim to learn a disease-related functional mapping matrix to form a functional profile that can be used to combine with brain structural network at later step. We will parameterize the representation of the similarity between two BOLD signals and the parameter will be automatically learned during the training process. The steps of the parameterization are presented as follows:

Averaged fMRI Signal Extraction: We used the Destrieux atlas (Destrieux et al. (2010)) to divide the whole brain into 148 regions. We calculated the average fMRI signal for each brain region as the representative for later analysis.

Normalization: We normalized the averaged fMRI signal using the standard Z-score normalization (Jain et al. (2005)) shown in (1),

$$f_i^* = \frac{f_i - f_\mu}{f_\sigma}, \tag{1}$$

where f_i is the averaged fMRI signal of brain region i, f_μ and f_σ are the mean and the standard deviation of all 148 averaged fMRI signals.

Functional Profile Learning: We defined the parameterized *functional-pairwise distance* between region-i and region-j using (2):

$$\phi\left(f_i^*,\ f_j^*; M\right) = M\left(f_i^* - f_j^*\right)^2,\ \forall\, i,\ j\ \varepsilon 1,\ \ldots,\ N, \tag{2}$$

where $M \in R^{T\times T}$ is the *learnable* functional mapping matrix, T is the number of time points of averaged fMRI signals. f_i^* and f_j^* are the normalized averaged signals of two brain regions. It is worth noting that the proposed parameterization approach (2) has been widely used in metric learning, where M is interpreted as a *linear* projection matrix and $\phi(f_i^*,\ f_j^*; M)$ becomes the Mahalanobis distance with precision matrix M^TM (Xing et al. (2003)). Different from conventional metric learning methods, we will integrate it into the proposed deep learning model with a natural *nonlinear* extension. Due to the high complexity of fMRI signals, linear projection function used in (2) is inadequate for modeling the distance/similarity of the averaged fMRI signals. To alleviate the above issue, nonlinear projection can be introduced by applying Gaussian kernel in terms of kernel trick given by

$$A_{ij}^F = \exp\left(-\frac{\phi\left(f_i^*,\ f_j^*; M\right)}{2\sigma^2}\right),\ \forall\, i,\ j\ \in 1,\ \ldots,\ N, \tag{3}$$

where$A_{ij}^F \in R$ represents the pairwise *functional profile* between brain region i and region j. $A^F\ \in R^{N\times N}$ is the matrix including all pairwise functional profiles between any two brain regions with the $(i, j)^{th} entry - -A_{ij}^F$, σ is the bandwidth parameter of Gaussian kernel and is treated as a hyper-parameter, which will be fully discussed in Section 4. In order to avoid introducing any bias, M is initialized as identity matrix. During the training process, M is iteratively updated based on classification results.

Brain Structure-Function Fusion

A major goal of this work is to examine MCI related network alterations via deep fusion of brain structural and functional data. To this end, we propose a novel strategy to integrate brain structural networks and functional profiles in a deep and regularized fashion. First, we calculate individual structural network matrix – $A^S \in R^{N\times N}$, which is a symmetric matrix and $A_{ij}^S \in R$ is the number of DTI-derived fibers connecting brain region i and region j. Then, we conduct normalization of A^S using (4) and (5). $(A^S)_\mu$ and $(A^S)_\sigma$ are the mean and the standard deviation of A^S. Because the number of fibers connecting two brain regions can be from zero to a few thousands and conform to a skewed distribution. Log transformation can equalize the standard deviations and make the distribution of the sample mean more consistent with a normal distribution (Curran-Everett (2018)). Therefore, we first used log transformation to narrow the range of the number of fibers by (4) and

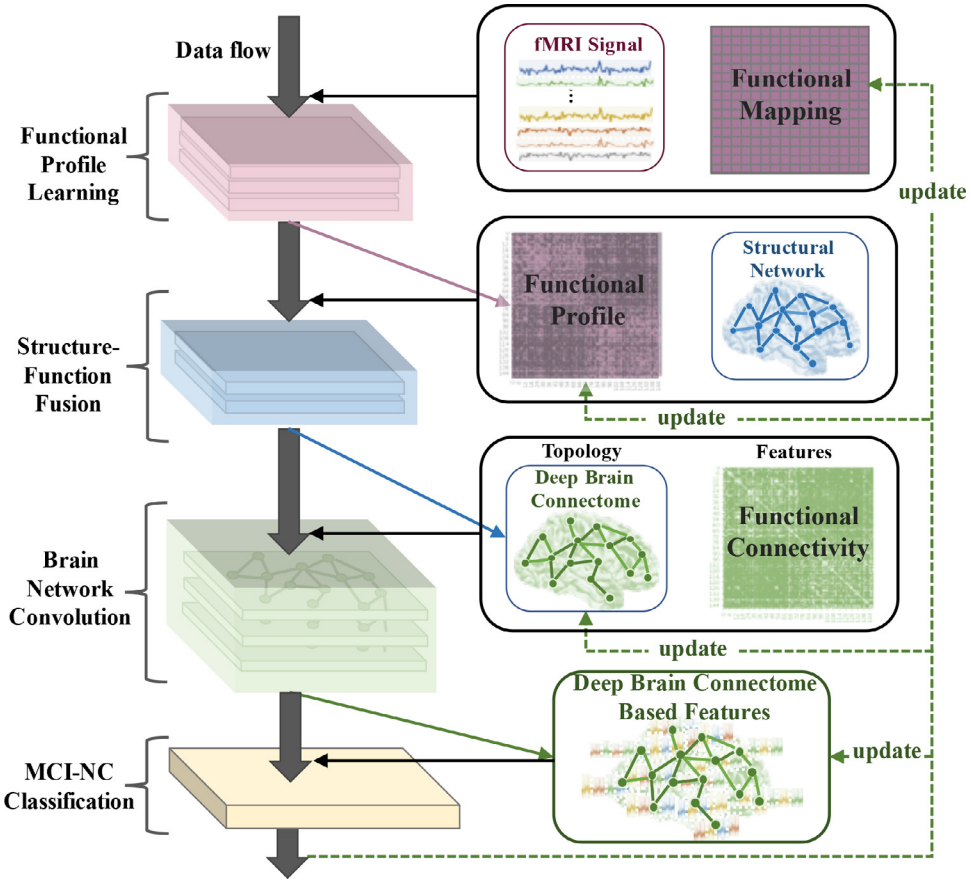

Fig. 2. The major steps of the proposed Graph Based Deep Model (GBDM). The model consists of four components: 1) functional profile learning, 2) brain structure-function fusion, 3) brain network convolution and 4) MCI-NC classification. Functional profile learning aims to learn a new representation of pairwise functional relations by introducing a trainable functional mapping matrix. In the step of brain structure-function fusion, structural network and the learned functional profile are combined as a hybrid brain network and it will be updated in each iteration. Using functional connectivity (defined with Pearson's correlation coefficient) as features associated to the network nodes (brain regions), we conduct graph convolution based on the hybrid brain network. A fully connected network is appended at last for MCI-NC classification and the results are used to update the parameters in previous layers. Because the learned hybrid brain network "deeply" integrates brain structure-function information to maximize its MCI-NC classification power, we name it as Deep Brain Connectome.

then used (5) for normalization.

$$A^S_{ij} = \log_{10}\left(A^S_{ij} + 1\right), \tag{4}$$

$$A^S = \frac{A^S - \left(A^S\right)_\mu}{\left(A^S\right)_\sigma}. \tag{5}$$

At last, we combine the normalized structural network (A^S) and functional profile (A^F) using (6) and (7):

$$\hat{A} = I + \theta_1 A^S + \theta_2 A^F, \tag{6}$$

$$\theta_k = \frac{\exp\left(-\beta_k\right)}{\sum_{m=1}^{2} \exp\left(-\beta_m\right)}, \tag{7}$$

where I is an identity matrix of $N \times N$ and it makes sure that each node can be considered in its own convolutional operations. θ_1 and θ_2 control the contributions of structural and functional components in the combined new brain connectome ($\hat{A}$). Here β_k ($k = 1, 2$) are introduced in (7) to constrain $\sum_{k=1}^{2} \theta_k = 1$ and $\theta_k > 0$. During this training process, θ_k is iteratively updated (via β_k) to improve the classification performance when differentiating MCI from NC in the fully connected layers (*Section 3.5*). It is clear that introducing β_ks in (7) can facilitate the gradient descend method to optimize θ_ks without cautious on the simplex constraint, and (7) is a continuous and differentiable function, which can be easily optimized by the backpropagation method. As a result, the presented fusion strategy is easily incorporated into our deep learning models. In general, the disease-related knowledge (from classification) is passed to functional profile (A^F) and then transferred to the new brain connectome ($\hat{A}$), by combining with structural network (A^S). This is an iterative process and at each iteration, $\hat{A}$ will be used as the new topology for graph convolution of node-associated features.

Brain Network Convolution

To represent the latent interactions in brain network, we adopt a multi-layer GCN architecture to fulfill the joint tasks of classification and brain connectome learning. GCN (Kipf & Welling (2016); Wu et al. (2020); Zhang et al. (2020b)) extends traditional CNN by applying convolutional operations on graph-based instead of Euclidean-based neighbors. Here we provide a basic definition of graph for better understanding of GCN.

Definition. A graph is denoted by $G = (N, E, A)$ where N is the set of nodes, E is the set of edges and $A \in R^{N \times N}$ is the adjacency matrix, N is the number of the nodes. In a graph, let $n_i \in N$ denote node i, $e_{ij} = (n_i, n_j) \in E$ denote an edge connecting n_i and n_j and $a_{ij} \in A$ to represent the connection strength between n_i and n_j.

For a graph G, each node n_i can have its own attributes represented by a row vector $x_i \in R^{1 \times D}$ and D is the dimension of attributes (features). $X = [x_1, \ldots, x_N] \in R^{N \times D}$ is the feature matrix of

the graph. We used the updated hybrid brain connectome $\hat{A}$ as the adjacency matrix in each iteration ($A = \hat{A}$). We calculated Pearson Correlation Coefficient of every pair of averaged fMRI signals as feature matrix $P \in R^{N\times N}$ ($X = P$). The feature vector of node n_i, $P_i = (P_{i1}, P_{i2}, \ldots, P_{iN})$, is the concatenation of correlations to all the other nodes. The input graphs in our model are individual-level graphs which have the same number of nodes representing the corresponding brain regions. More importantly, the topology of the graphs ($A = \hat{A}$) are flexible and will be iteratively updated in the training process to maximize its classification power when differentiating MCI from NC.

Graph Spectral Convolution: given a graph G = (N, E, A) and the feature matrix $X = \{x_i \in R^{N\times D}\}_{i=1}^{N}$, the spectral convolutions on graphs was defined as $g_\theta * x_i = U g_\theta U^T x_i$ in the Fourier domain. $g_\theta = \mathrm{diag}(\theta)$ is a filter parameterized by a vector of Fourier coefficients $\theta \in R^N$. U is a set of eigenvectors of normalized graph Laplacian $L = I_N - \mathcal{D}^{-\frac{1}{2}} A \mathcal{D}^{-\frac{1}{2}} = U\mathbf{\Lambda}U^T$, where $\mathcal{D}$ is the degree matrix of A, $\mathbf{\Lambda}$ is a diagonal matrix of the corresponding eigenvalues and g_θ can be viewed as a function of the eigenvalues, i.e. $g_\theta(\mathbf{\Lambda})$. $U^T x_i$ is the graph Fourier transform of x_i. The complexity of calculating $U g_\theta U^T x_i$ is $O(N^2)$ and computing the eigen-decomposition of graph Laplacian$L$ is prohibitively expensive for large graphs. To solve this problem, in Michaëlet al. (2016) $g_\theta(\mathbf{\Lambda})$ is formulated as a polynomial: $g_\theta(\mathbf{\Lambda}) = \sum_{k=0}^{K-1} \theta_k \mathbf{\Lambda}^k$. This is a K-localized kernel since the filter is represented by the K^{th}-order polynomial of the graph Laplacian, which depends only on nodes within K steps (K^{th}-order neighborhood) away from the central node. The complexity of calculating $\sum_{k=0}^{K-1} \theta_k \mathbf{\Lambda}^k$ is $O(|E|)$, which is linear with the number of the edges. A graph convolutional network can be built by stacking multiple convolutional layers of the polynomial form: $g_\theta(\mathbf{\Lambda}) = \sum_{k=0}^{K-1} \theta_k \mathbf{\Lambda}^k$. For example, in Kipf & Welling (2016), a two-layer GCN is formulated by $Z = f(X, A) = f(\hat{A}\, ReLU(\hat{A}XW^{(0)})W^{(1)})$, where $\hat{A} = \mathcal{D}^{-\frac{1}{2}} A \mathcal{D}^{-\frac{1}{2}}$ is the Laplacian transformation of A. In our previous work (Zhang et al. (2019)), we evaluated $\hat{A} = A$ and other three different Laplacian transformations of A: $\hat{A} = \mathcal{D} - A$, $\hat{A} = \mathcal{D}^{-\frac{1}{2}} A \mathcal{D}^{-\frac{1}{2}}$, and $\hat{A} = \mathcal{D}^{-1}A$. We found that $\hat{A} = A$ and $\hat{A} = \mathcal{D}^{-\frac{1}{2}} A \mathcal{D}^{-\frac{1}{2}}$ give similar classification performances. Thus, in this work we used the matrix calculated by (6) directly without Laplacian transformation. The advantages are as follows: 1) compared to $\hat{A} = \mathcal{D}^{-\frac{1}{2}} A \mathcal{D}^{-\frac{1}{2}}$, $\hat{A} = A$ needs less computational cost; and 2) in this work, we attempt to explore the structural and functional network alterations in MCI patients, extra transformation on the original data may have unknown influence on the results.

Based on above discussion, in this work the convolutional process of multi-layer graph convolutional network is formulated by (8) and (9).

$$G = f\left(\hat{A}H^{l-1}W_l\right), \tag{8}$$

$$H^l = \begin{cases} f\left(\hat{A}H^{l-1}W_l\right), & l \geq 1, \\ P, & l = 0, \end{cases} \tag{9}$$

where f is the nonlinear activation function and we used *Relu* in our experiment. For the l^{th} layer, H^l is the output, $W_l \in R^{F_{li}\times F_{lo}}$ is the weight matrix, F_{li} and F_{lo} are the feature sizes of input and output feature matrix. As showed in Fig. 3, each W_l is a filter which selects related features from neighbors and defines how to combine these features. By stacking multiple graph convolutional layers, information from high-order neighbors (indirectly connected via other nodes) can be propagated along brain connectome defined by current adjacency matrix $\hat{A}$. Fig. 4 illustrates the neighbors with different order and how a multi-layer GCN conducts the graph convolution at different layers. Our previous study (Zhang et al. (2020a)) suggested that the impact of MCI-related alterations may go beyond the first-order neighbors and be limited to the third-order neighbors. Therefore, in our experiments, brain network based convolutions were implemented using a two-layer GCN.

MCI-NC Classification

In the last part of GBDM, we designed a two-layer fully connected neural network to perform binary classification for two classes – MCI and NC. Based on the classification performance, the gradient information will be propagated back to the entire network and the following parameters will be updated accordingly: 1) $\{W_l\}$ in brain network convolution – *Section 3.4*; 2) $\{\theta_k\}$ in brain structure-function fusion – *Section 3.3*; and 3) M in functional profile learning – *Section 3.2*. Through this way, the disease-related knowledge drives the training process to learn a new brain connectome – $\hat{A}$ (*see (6)*) which represents a deep fusion of brain structure and function, that is the *deep brain connectome*. After the above three parameters are obtained after training process, we can make prediction for any given individual data including structural network matrix A^S, feature matrix P, and averaged fMRI signals $\{f_i\}$: the first step is to calculate the individual deep brain connectome $\hat{A}$ by using (6) and the optimized M and $\{\theta_k\}$; then P together with $\hat{A}$ are forward propagated through the trained deep graph convolutional network with optimized $\{W_l\}$ to the classification layer for final prediction.

Results

We applied our proposed GBDM to individual fMRI signals and brain structural network. For each sample (subject) in training data, the individual structural network is used to initialize the adjacency matrix with (6). Individual functional signals are used for functional profile learning (*see (3)*), brain structure-function fusion (*see (6)*) as well as node features in (9). Besides classification, the major outcome of GBDM is the learned hybrid connectome – deep brain connectome ($\hat{A}$), which integrates the knowledge from both brain structural and functional data. In the results, Section 4.1 and 4.2 introduce the participants and data preprocessing. Section 4.3 shows the experimental setting. Section 4.4 shows the comparison of classification performance with other widely used methods. Section 4.5 shows the details of the learned deep brain connectome and the evaluation of different model settings will be discussed in Section 4.6.

Participants

In this work, we jointly analyzed three modalities of brain imaging data in ADNI dataset, including structure MRI (T1-weighted), resting state fMRI (rs-fMRI) and DTI. We began with 252 subjects (132 Normal Controls (NC) and 120 MCI patients) which have all three modalities. 38 (16 NC and 22 MCI) subjects were not used in this work due to poor image quality. In total, we have 214 subjects including 116 subjects from NC group (60 females, 56 males; 74.26 ± 8.42 yrs.) and 98 subjects from MCI group (57 females, 41 males; 74.23 ± 8.81 yrs.). The proposed analysis was conducted on these 214 subjects.

Data Description and Preprocessing

The T1-weighted MRI data has 240 × 256 × 208 voxels and the voxel size = 1.0 mm × 1.0 mm × 1.0 mm, TR = 2.3s. The DTI data has 54 gradient directions, each volume has 116 × 116 × 80 voxels and the voxel size = 2.0 mm × 2.0 mm × 2.0 mm, TE = 56ms and TR = 7.2s. The rs-fMRI data has 197 volumes, each volume has 64 × 64 × 48 voxels and the voxel size = 3.4375 mm × 3.4375

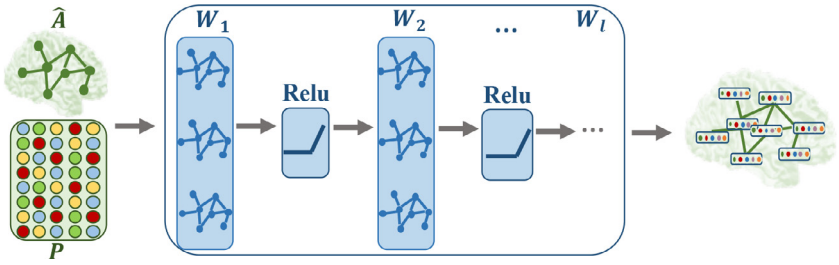

Fig. 3. Multi-layer graph convolutional network. According to the input adjacency matrix $\hat{A}$ and feature matrix P, a GCN layer creates a hidden representation for each node by combining features from its neighbor nodes based on W_l. After the combination, a nonlinear transformation is applied to the hidden representation. By stacking multiple layers, the final hidden representation of each node gathers information from both direct neighbors and high-order neighbors (indirectly connected via other nodes).

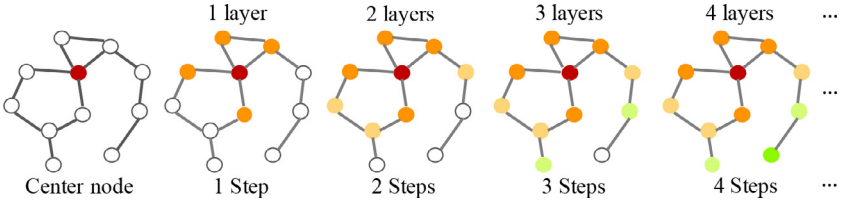

Fig. 4. The influences of using different numbers of GCN layers for aggregating features. We use step to represent the number of edges in a shortest path connecting two nodes in the graph. The nodes with the same color represent that they have the same steps from the center node (red). With more GCN layers are stacked the deeper of brain network relations are considered.

mm × 3.4 mm, TE = 30ms, TR = 3s and flip angle = 90°. The first 6 volumes were discarded during preprocessing procedures to ensure magnetization equilibrium.

We applied the same standard preprocessing procedures as in Zhu et al. (2014a) and Wang et al. (2019). In brief, we applied skull removal for all modalities. For rs-fMRI images, we applied spatial smoothing, slice time correction, temporal pre-whitening, global drift removal and band pass filtering (0.01-0.1 Hz). All of these preprocessing steps are implemented using FMRIB Software Library (FSL) (Jenkinson et al. (2012)) FEAT. For DTI images, we applied eddy current correction via FSL and fiber tracking via MedINRIA. For T1-weighted images, we registered them to DTI space by FSL FLIRT and then conducted segmentation using FreeSurfer package (Fischl (2012)). After the segmentation, we adopted the Destrieux Atlas (Destrieux et al. (2010)) for ROI labeling and the brain cortex is partitioned into 148 regions after removing two unknown areas and two empty areas.

Experimental Setting

Data Setting. For each subject, the whole brain is divided into 148 regions using Destrieux Atlas. We calculate averaged fMRI signal for each brain region and created brain structural network (A^S) and Pearson Correlation Coefficient matrix (P) for each subject. For classification, we conducted 5-fold cross-validation using the 214 subjects (116NC/98MCI).

Model Setting. The functional profile learning was implemented by one fully connected layer with the input dimension and the output dimension of T, where T is the number of time points. We employed a two-layer GCN for brain network convolution. The output feature dimensions of the first GCN layer and the second GCN layer are 148 and 296, respectively. The two feature dimensions are selected according to model evaluation (*Section 4.6*). The MCI-NC classification was conducted by one fully connected layer with input dimension 43808 (region number (148) × feature size (296)) and output dimension C, where C is the number of classes (C=2 in this work). The entire model was trained in an end-to-end manner. During the training process, the parameters were initialized following the Xavier scheme. The Adam optimizer was used to train the whole model with standard learning rate 0.0005, weight decay 0.01, and momentum rates (0.9, 0.999).

Classification Performance

The proposed GBDM is based on MCI/NC classification task. In this section, we focus on comparing classification performance of the proposed method with other widely used methods. As mentioned earlier, GBDM is designed to learn a deeply combined structural-functional connectome that can be used to achieve higher MCI/NC classification performance. For fairly comparison, we summarize the overall classification performance of recent MCI studies using both single-modality and multi-modality as well as our model in Table I. The approaches of classification include traditional machine learning methods, such as SVM (Min et al. (2014); Cheng et al. (2015); Dyrba et al. (2015); Liu et al. (2015); Möller et al. (2016); Shao et al. (2020) and most recent deep learning models, such as CNN (Aderghal et al. (2018); Liu et al. (2018); Huang et al. (2019)). The single modality includes MRI, DTI, and PET. The multi-modality includes MRI + PET, MRI + PET + biomarkers, MRI + PET + biomarkers + Genetics, MRI + DTI, and MRI + DTI + fMRI. For AD/NC classification, the accuracy of most single-modality methods listed in Table 1 is bellow 90% while the accuracy of most multi-modality methods is over 90%. Although the performance of Min et al. (2014) and Liu et al. (2015) stand out than other listed single-modality methods and can reach an accuracy over 90%, they used multi-view and multi-atlas to organize the single-modality data at different scales and different views. For MCI/NC classification, the accuracy of most single-modality methods is bellow 80% while the accuracy of most multi-modality methods is over 80%. Among the listed studies, Aderghal et al. (2018), Liu et al. (2018) and Shao et al. (2020) tested the proposed methods with both single-modality and multi-modality. Their results indicate that comparing to single-modality, using multi-modality data can achieve higher classification accuracy. Some of the listed multi-modality methods used PET data, which inclines to have better classification power than MRI based modalities. It is worth noting that our method used noninvasive DTI/fMRI data and achieves the best performance of 92.7% for MCI/NC classification. Our result suggests that recognition of the complex relationship between different modalities may be critical for better understanding brain structure-function alterations in brain disorder studies.

Table 1
Performance Comparison of Different Methods in AD/MCI Classification.

(A) Single-Modality Study

Study	Modality	Group			Method	Accuracy (%)			
		AD	MCI	NC		AD/NC	MCI/NC	AD/MCI	pMCI/sMCI
Apostolova et al. (2014)	MRI	95	182	111	Hippocampus; SVM	85.0	79.0	70.0	-
Min et al. (2014)	MRI	97	$117^{p}+117^{s}$	128	Multi-atlas; Morphometry; SVM	91.6	-	-	72.4
Liu et al. (2015)	MRI	97	$117^{p}+117^{s}$	128	multi-view; multi-template; SVM	93.8	-	-	80.9
Möller et al. (2016)	MRI	84	-	94	Gray matter density maps; SVM	88.0	-	-	-
Aderghal et al. (2018)	MRI	188	399	228	Hippocampus; CNN; transfer learning	90	72.5	82.5	-
Aderghal et al. (2018)	DTI	48	108	58	Hippocampus; CNN; transfer learning	85	62.5	82.5	-
Liu et al. (2018)	MRI	93	$76^{p}+128^{s}$	100	Patch-based; Cascaded CNNs	85.0	77.8^{p} 60.1^{s}	-	-
Liu et al. (2018)	PET	93	$76^{p}+128^{s}$	100	Patch-based; Cascaded CNNs	88.1	78.4^{p} 63.4^{s}	-	-
Shao et al. (2020)	MRI	160	$273^{e}+187^{l}$	160	Hypergraph; Multi-kernel SVM	88.3	69.1	-	68.5
Shao et al. (2020)	PET	160	$273^{e}+187^{l}$	160	Hypergraph; Multi-kernel SVM	87.3	65.6	-	67.6

(B) Multi-Modality Study

Study	Modality	Group			Method	Accuracy (%)			
		AD	MCI	NC		AD/NC	MCI/NC	AD/MCI	pMCI/sMCI
Dyrba et al. (2015)	MRI+DTI+fMRI	28	-	25	ROI-based; Multi-kernel SVM	79.0	-	-	-
Cheng et al. (2015)	MRI+PET+ biomarkers	51	$43^{p}+56^{s}$	52	ROI-based; Doman transfer SVM	-	86.4	82.7	79.4
Yu et al. (2016)	MRI+PET+ biomarkers	50	97	52	ROI-based; Graph-guided learning	92.6	80.0	-	-
Shi et al. (2017)	MRI + PET	51	$43^{p}+56^{s}$	52	ROI-based; Multimodal SDPN	97.1	87.2	-	78.9
Tong et al. (2017)	MRI+PET+ biomarkers+ Genetics	37	75	35	Nonlinear Graph-fusion;	91.8	79.5	-	-
Aderghal et al. (2018)	MRI+DTI	48	108	58	Hippocampus; CNN; Transfer learning	92.5	80	85	-
Liu et al. (2018)	MRI+PET	93	$76^{p}+128^{s}$	100	Patch-based; Cascaded CNNs	93.3	83.0^{p} 64.0^{s} 74.3	-	-
Huang et al. (2019)	MRI+PET	647	$326^{p}+441^{s}$	731	Hippocampus; CNN	90.1	87.5^{p}	-	76.9
Peng et al. (2019)	MRI+PET+ Genetics	49	93	47	Structured sparsity; Kernel representation	96.1	80.3	76.9	-
Zheng et al. (2019)	MRI+PET	-	$51^{p}+75^{s}$	-	Connectivity-based; Multi-task regression	-	-	-	79.4
Shao et al. (2020)	MRI+PET	160	$273^{e}+187^{l}$	160	Hypergraph; Multi-kernel SVM	92.5	82.5	-	75.48
Proposed	MRI+DTI+fMRI	-	98	116	GBDM	-	92.7	-	-

Group: $a^{e}+b^{l}$: the number of EMCI is a and the number of LMCI is b; $c^{p}+d^{s}$: the number of pMCI is c and the number of sMCI is d.
Accuracy (%): a^{p}: the accuracy of CN/pMCI is a; b^{s}: the accuracy of CN/sMRI is b.

Deep Brain Connectome

Besides classification of MCI patients, the other major outcome of GBDM is the learned deep brain connectome ($\hat{A}$). By comparing the learned deep brain connectome with the original brain structural network, we are able to examine the functional influences on the structural connectivity (fusion of structural and functional data) when conducting MCI classification task. All the results showed in this section are based on the testing dataset.

Overall patterns of deep brain connectome

After applying the trained GBDM to each testing subject, the individual deep brain connectome – $\hat{A}$ can be computed via (6). The difference between $\hat{A}$ and the structural network reflects the influence of functional data in the deep structure-function fusion when classifying MCI from NC. Therefore, we are interested with the changed connectivity of $\hat{A}$ comparing to the corresponding structural network. Fig. 5 (a) shows the averaged results of different groups: NC and MCI. For each matrix, the order of the brain regions is the same as the order defined in Destrieux atlas (Destrieux et al. (2010)): the upper left/lower right represents the connectivity within the same hemisphere and the connections between different hemispheres are located in upper right/lower left. The first column displays the group-wise structural network and we can see that the overall patterns of two groups are similar: they show relatively stronger fiber connections in the same hemisphere (Tsai (2018)). The second column shows the obtained deep brain connectome. Through visual examination we can find that comparing to the structural network, the deep brain connectome is decreased within the same hemisphere and increased across different hemispheres. These interesting results suggest that after incorporating functional data to structural network, some cross-hemisphere connectivity are strengthened to improve the classification power in deep brain connectome. To better demonstrate the inter- and intra- hemisphere patterns, we showed the increased

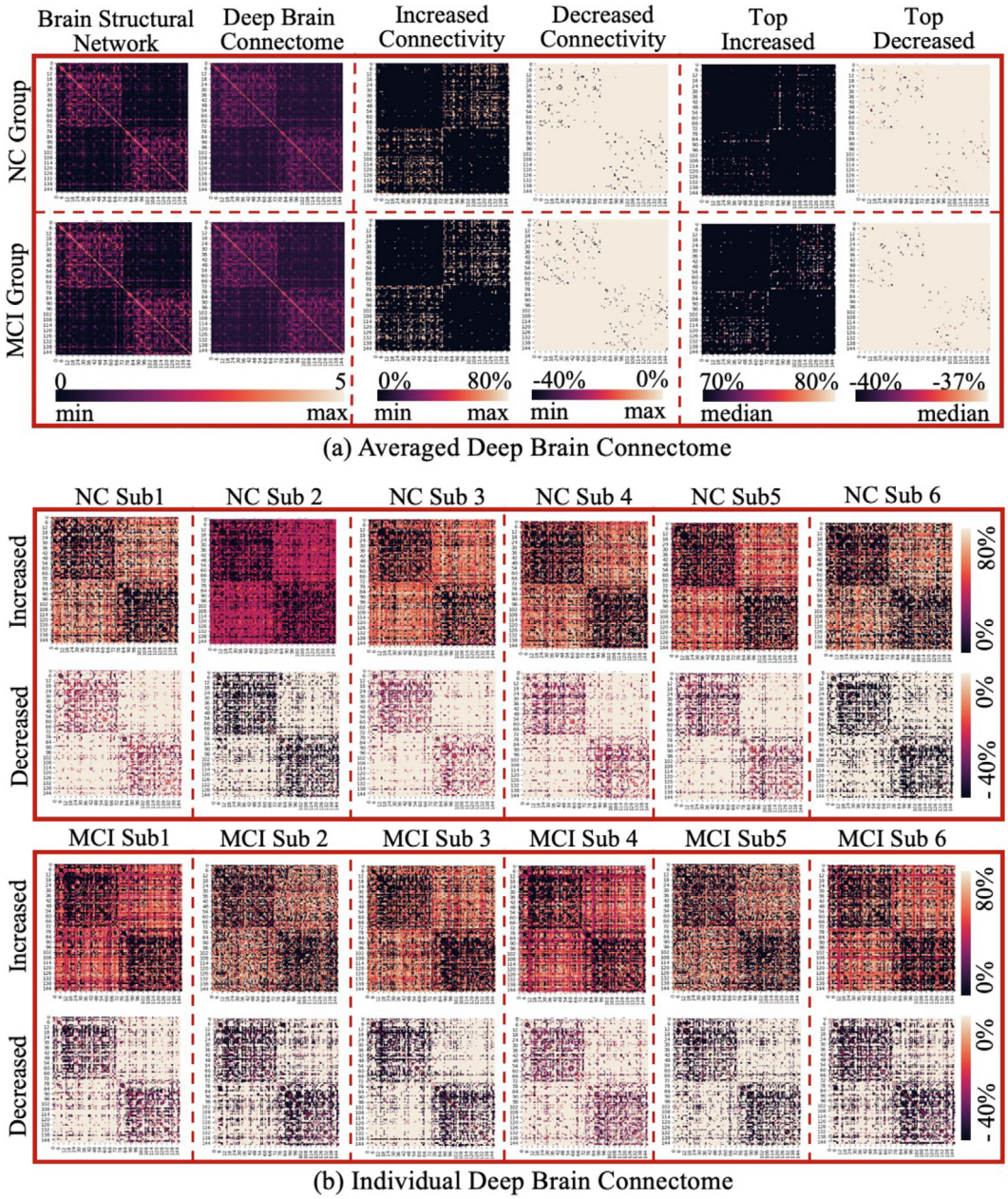

Fig. 5. The results of the learned Deep Brain Connectome and comparison with brain structural network. (a) shows the averaged results for NC group (the first row) and MCI group (the second row). For each group, the first column displays the group-wise structural network and the order of the brain regions listed in the matrix is the same as Destrieux atlas. The second column shows the learned deep brain connectome. Compared to brain structural network, the increased and decreased connectivity in deep brain connectome are shown in the third and fourth column. The top changed connectivity using the thresholds of 70% (for increased connectivity) and 37% (for decreased connectivity) are shown in the fifth and sixth column. (b) shows the increased and decreased connectivity of 6 randomly selected subjects from NC group (the first block) and MCI group (the second block).

and decreased connectivity separately at the third and the fourth columns in Fig. 5 (a). We can see that the increased connectivity is mostly composed of the ones connecting to different hemispheres (the third column), while the decreased connectivity is located within the same hemisphere (the fourth column). Note that in order to improve the robustness and exclude the potential noisy data, we only consider the increased/decreased connectivity which have changed by more than 5% on every subject in the testing dataset. Besides the averaged results, we also randomly selected 6 subjects from testing dataset for each group and showed the individual increased and decreased connectivity in Fig. 5 (b). The patterns of the altered connectivity of single subject are consistent with the averaged results. Moreover, we used medians of the changes (70% for increased and 37% for decreased) as the thresholds to select the top increased and decreased connectivity and showed them in the fifth and the sixth columns in Fig. 5 (a). Our results indicate that the number of top increased connectivity in MCI group is much more than that in NC group. To further analyze the group level differences, we examine the distribution of the changed connectivity in deep brain connectome based on the changing scale.

Changed connectivity in deep brain connectome

To further study the changed connectivity in deep brain connectome and better illustrate the group level differences, we calculated the distribution regarding the changing scale of increased and

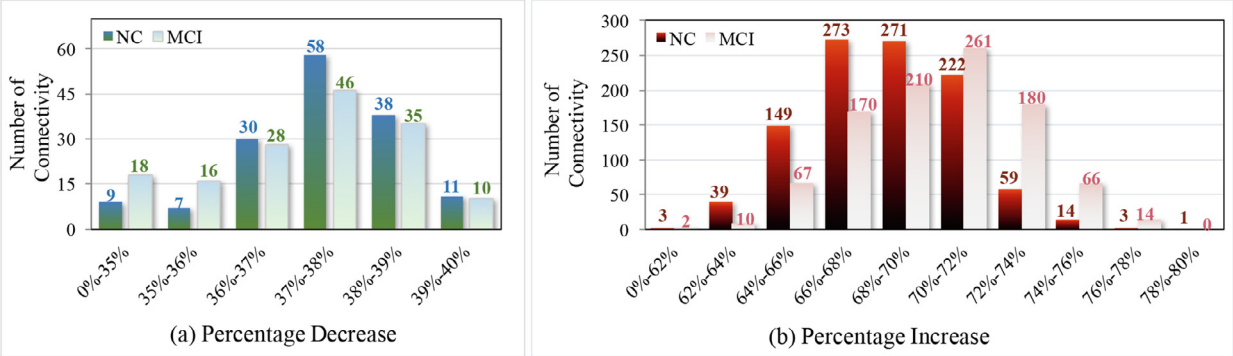

Fig. 6. Changing rate (%) for the increased connectivity ((a)) and decreased connectivity ((b)) of NC and MCI groups.

Table 2
Top 10 Increased Connectivity.

NC			
Connection	Change	Connection	Change
lh_Pole_temporal rh_G_front_inf-Orbital	78%	lh_S_temporal_sup rh_G_front_inf-Orbital	77%
lh_G_temp_sup-Plan_polar rh_G_front_inf-Orbital	77%	lh_G_temporal_middle rh_G_front_inf-Orbital	77%
lh_S_precentral-sup-part rh_G_Ins_lg&S_cent_ins	76%	lh_G_pariet_inf-Supramar rh_G_front_inf-Orbital	75%
lh_S_circular_insula_ant rh_G_front_inf-Orbital	75%	lh_Lat_Fis-post rh_G_front_inf-Orbital	75%
lh_G&S_subcentral rh_S_central	75%	lh_S_precentral-inf-part rh_G_front_inf-Orbital	75%
MCI			
Connection	Change	Connection	Change
rh_G_cuneus rh_Lat_Fis-post	78%	rh_S_precentral-sup-part rh_S_temporal_transverse	77%
part lh_S_central rh_S_collat_transv_post	77%	lh_G_temp_sup-G_T_transv rh_S_precentral-sup-	77%
lh_G_front_sup rh_S_temporal_transverse	77%	lh_G_temp_sup-Plan_tempo rh_S_precentral-sup-part	77%
lh_S_temporal_transverse rh_S_precentral-sup-part	77%	lh_S_precentral-sup-part rh_G_cuneus	76%
lh_G_temp_sup-Plan_temprh_Lat_Fis-ant-Vertical	76%	lh_G_temp_sup-Plan_temporh_G&S_cingul-Mid-Post	76%

decreased connectivity (Fig. 6). For both NC and MCI groups, there are more increased connectivity (NC=1034, MCI=980 and 2014 in total) than decreased connectivity (NC=153, MCI=153 and 306 in total). The scale of changing for decreased connectivity mainly ranges from 35% to 40%, whereas increased connectivity has higher percentage of changing which is from 62% to 80%. The increased connectivity inclines to possess larger changing scale than the decreased ones. Another observation is that for increased connectivity, the changing scale of MCI group is higher than NC group.

Visualization of the brain regions involved in the top changed connectivity

For better visualizing the changed connectivity and the related brain regions, we adopt two strategies to project them back to brain space. We first show the top 10 increased and decreased connectivity with the largest changing scale for MCI and NC groups in Fig. 7 (a). It is consistent with Fig. 5 that the increased connectivity are mainly the ones connecting the regions on different hemispheres and the decreased connectivity are located within the same hemisphere. In addition, the top increased connectivity inclines to connect brain regions with long distance, while decreased ones mostly connect local areas. We list the top 10 changed connectivity, involved brain regions as well as the percentage of changes in Table 2 and Table 3.

The second way to project the changed connectivity is using the same threshold for the level of changing compared to the initial structural network. Here, to better demonstrate the differences between NC and MCI groups and the differences between increased and decreased connectivity, we used 72% (for increased connectivity) and 38% (for decreased connectivity) and the results are shown in Fig. 7 (b). For both MCI and NC groups, the number of increased connectivity is much more than the decreased ones. This implicates that to improve the classification performance, the learned deep connectome enhanced many structural connectivity by deep fusion of structural and functional data. Moreover, with the same threshold MCI group shows much more increased connectivity than NC group. We summarized all the brain regions that are involved in the top connectivity in Table S1 and Table S2 in Supplementary.

Model Evaluation

There are two key hyper-parameters in the proposed GBDM that may affect our results. The first is the σ in (3), which controls functional profile learning. The second parameter is the dimension of the output features at each graph convolutional layer, which directly affects graph convolution. In this paper, we used G (F_1, F_2) to denote the architecture of graph convolutional network and F_l is the dimension of the output features at the l^{th} convolutional layer. Since the dimension of the input data is 148 $\times$ 148, we will evaluate the influence using different feature dimensions $F_l = 148 * a$, ($a = 1, 1.5, 2, \ldots, 6$). For each model setting we conducted 5-fold cross-validation using the same input data. The influences of the two hyper-parameters on classification performance, overall patterns of the changed connectivity and the scale of changing are discussed in this section.

Influence on classification performance

Because the proposed GBDM is driven by the classification results, we firstly evaluate the influence of σ and feature dimensions on classification performance. We tried a spectrum of σ (from 1.0 to 3.0) with different feature dimensions (from (148, 296) to (444, 888)) and showed the classification performance in Table 4. In

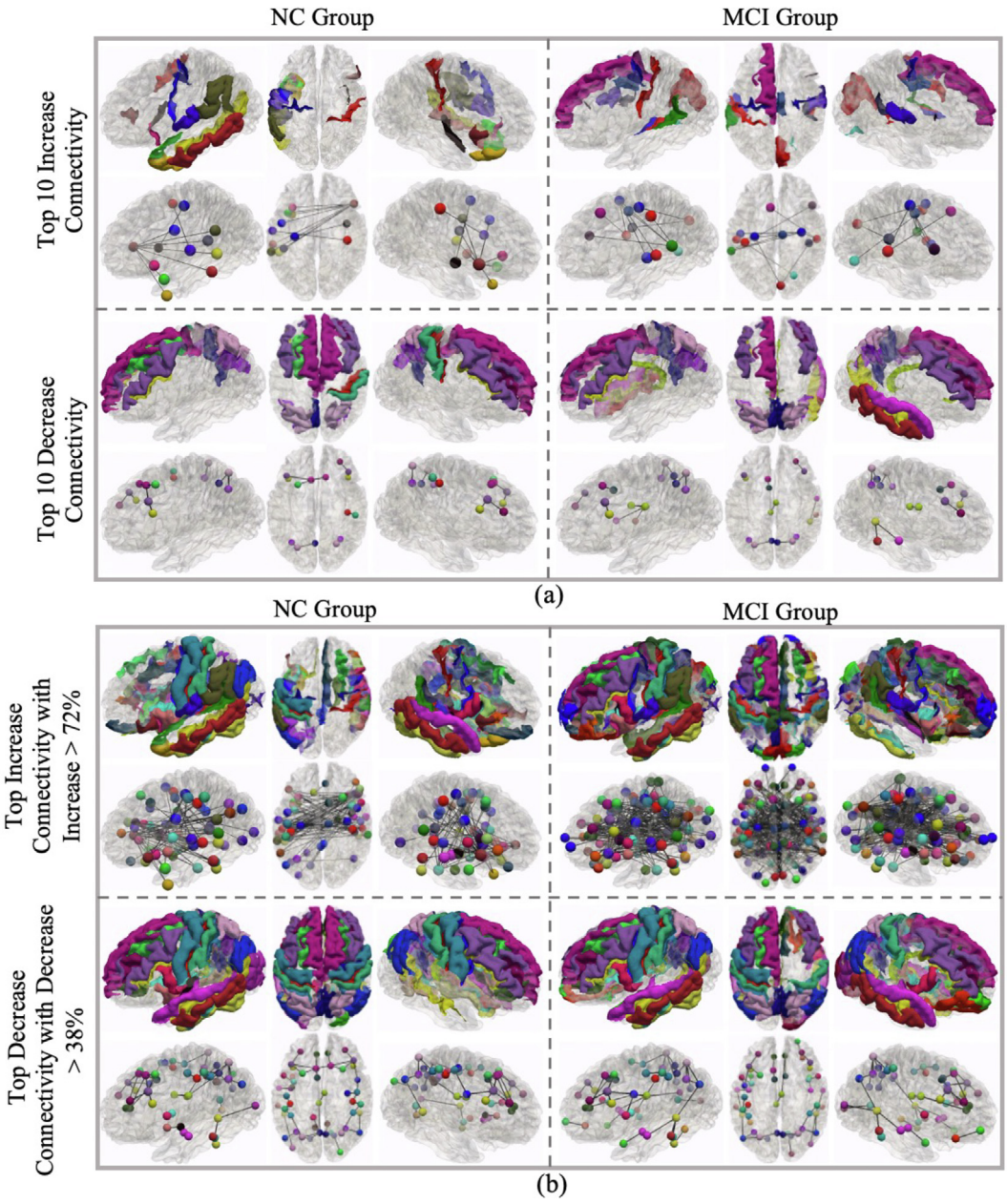

Fig. 7. The top increased/decreased connectivity and the involved brain regions for both MCI and NC groups. (a) shows the brain regions related to the top 10 increased and decreased connectivity and their connections. (b) shows the brain regions related to the increased and decreased connectivity with an averaged changing rate above 72% and 38%, respectively. For subfigures in both (a) and (b), the first row shows the involved regions and the second row highlights the regions as colored bubbles as well as the connections.

order to evaluate the classification performance in a more comprehensive way, we summarized accuracy (Acc), averaged precision (Pre), averaged recall (Rec), and averaged specificity (Spec) for each model setting. For accuracy, we showed the best, worst, and averaged results separately. The combination of $\sigma = 2.0$ with G (148, 296) gives the best accuracy – 92.7%. The other settings also showed decent performance in this work. In general, our proposed GBDM performs relatively stable within a wide range for the two key parameters.

Influence on the patterns of the changed connectivity

To demonstrate the influence of different parameters on the changed connectivity in deep brain connectome, we displayed the top increased and decreased connectivity obtained under different model settings in Fig. 8. In general, the patterns of the changed connectivity are very consistent: though the number and scale of the changed connectivity may be slightly different with different σ and feature dimensions, the top increased and decreased connectivity display the same inter- and intra- hemisphere patterns as Fig. 5. Here we only showed the top changed connectivity, the complete comparison including structural network, deep brain connectome and the changed connectivity can be referenced in Fig. S1 and Fig. S2 in Supplementary.

Influence on the scale of the changed connectivity

Here we will discuss the influence of σ and feature dimension on the scale of the changed connectivity. We projected the

Table 3
Top 10 Decreased Connectivity.

NC			
Connection	Change	Connection	Change
lh_G_front_sup rh_G_front_sup	40%	lh_G_front_sup lh_S_front_sup	39%
lh_G_parietal_sup lh_G_precuneus	39%	rh_G_front_middle rh_S_front_middle	39%
rh_G_parietal_sup rh_S_intrapariet&P_trans	39%	lh_G_front_middle lh_S_front_inf	39%
lh_G_parietal_sup lh_S_intrapariet&P_trans	39%	lh_G_front_middle lh_G_front_sup	39%
rh_G_front_middle rh_S_front_inf	39%	rh_G_postcentral rh_S_central	39%
MCI			
Connection	Change	Connection	Change
rh_G_parietal_sup rh_S_intrapariet&P_trans	40%	lh_G_front_middle lh_S_front_inf	40%
rh_G_parietal_sup rh_G_precuneus	40%	rh_G_temporal_middle rh_S_temporal_sup	40%
lh_G_parietal_sup lh_G_precuneus	39%	lh_G_parietal_sup lh_S_intrapariet&P_trans	39%
rh_G_temp_sup-Lateral rh_S_temporal_sup	39%	rh_G_front_middle rh_S_front_middle	39%
lh_S_pericallosal rh_S_pericallosal	39%	lh_G&S_cingul-Mid-Ant lh_G_front_sup	39%

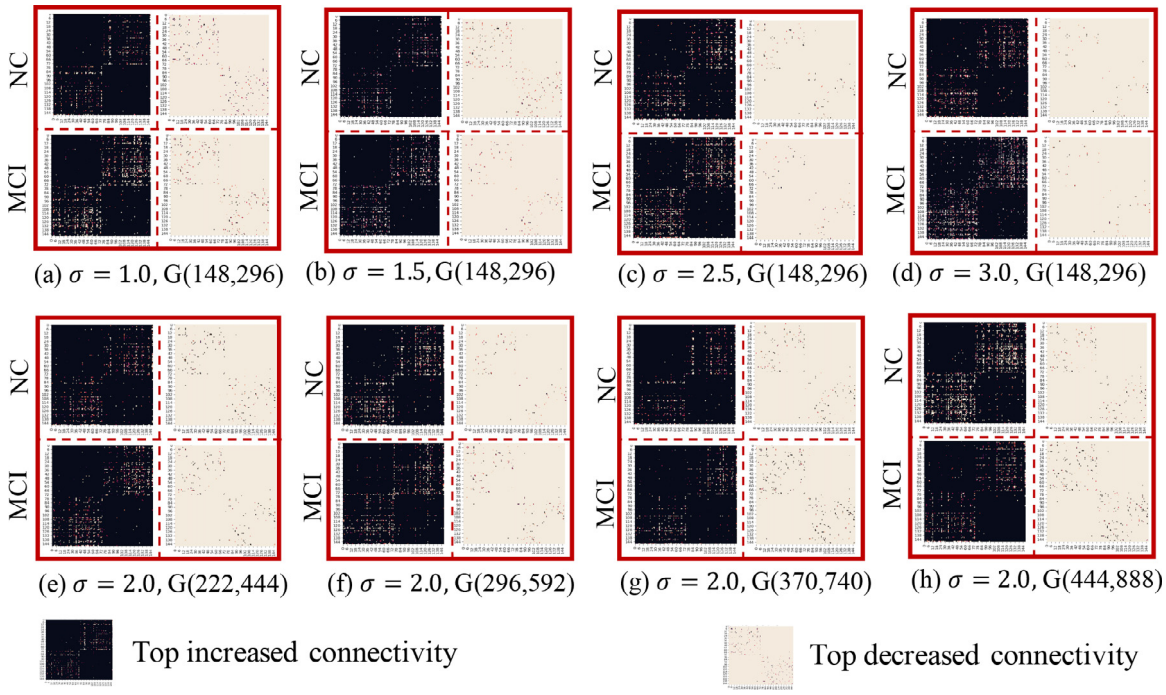

Fig. 8. Top increased and decreased connectivity under different model settings. We used different combinations of σ and feature dimension to conduct our experiments. The complete comparison including structural network, deep brain connectome and the changed connectivity are shown in Fig. S1 and Fig. S2 in Supplementary.

Table 4
Classification Performance under Different Model Settings.

Model Setting	Performance (%)						
Feature Dimension	σ	Acc[a]			Pre[b]	Rec[c]	Spec[d]
		Best	Worst	Ave[e]			
G(148, 296)	1.0	87.4	82.9	84.2	85.5	75.7	90.4
G(148, 296)	1.5	89.3	84.5	87.1	83.1	90.8	84.0
G(148, 296)	2.0	92.7	83.3	86.3	85.7	80.6	89.9
G(148, 296)	2.5	86.6	79.6	83.6	86.2	74.7	88.3
G(148, 296)	3.0	89.5	81.3	85.9	84.1	80.3	90.2
G(222, 444)	2.0	85.9	78.9	83.6	82.4	83.6	83.5
G(296, 592)	2.0	84.3	79.8	82.9	88.7	72.3	92.0
G(370, 740)	2.0	88.8	81.4	84.7	90.2	83.3	93.0
G(444, 888)	2.0	90.2	87.3	89.1	82.8	89.8	88.7

[a]Acc = Accuracy, [b]Pre = Precision, [c]Rec = Recall, [d]Spec = Specificity, [e]Ave = Average

trends of maximum and median values of the changing scale in Fig. 9. Fig. 9 (a) shows the impact of σ with fixed feature dimension. It is obvious that as σ becomes larger, both the maximum and the median of the changing scale for increased connectivity become larger, while the decreased connectivity inclines to change less. One reason is that according to (3) the learned functional profile A^F is positive proportional to σ. Thus, a larger σ leads to an A^F with larger values. Because A^F contributes to the partial differences between structural connectivity and deep brain connectome – $\hat{A}$, the change of σ will affect the scale of the changed connectivity. Even so, more than 83% of the brain regions associated with the top 100 changed connectivity are still the same. Fig. 9 (b) shows the impact of feature dimension with fixed σ. The maximum and median of the changing scale for both increased and decreased connectivity are similar across different model settings. These results suggest that the dimension of the output features seems less sensitive than the other hyper-parameter – σ.

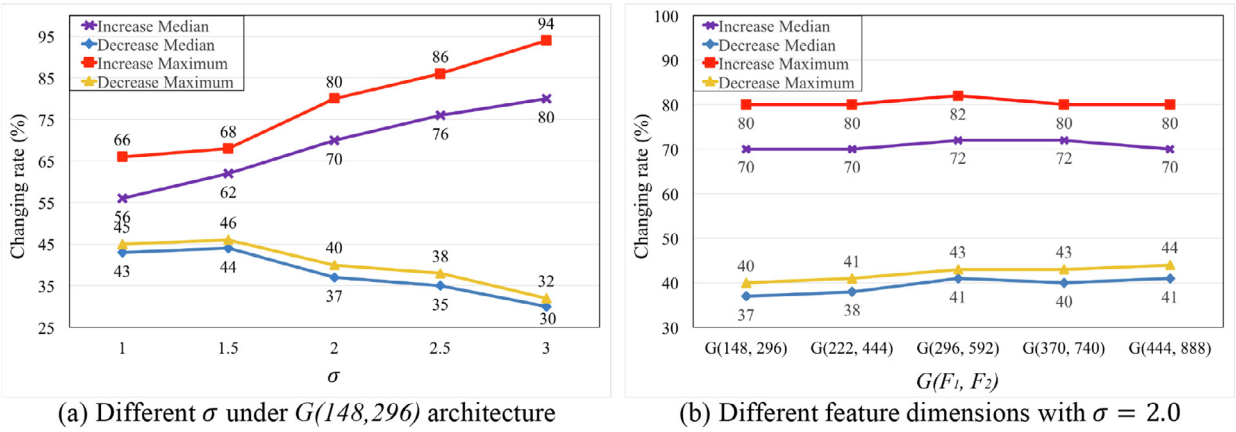

(a) Different σ under $G(148,296)$ architecture (b) Different feature dimensions with $\sigma = 2.0$

Fig. 9. Influence of σ and feature dimension on changing scale of the altered connectivity. (a) shows the maximum and median of changing rate of the increased and decreased connectivity with a spectrum of σ (from 1.0 to 3.0) based on G(148, 296). (b) shows the maximum and median of changing scale of the increased and decreased connectivity of different feature dimensions with the same $\sigma = 2.0$.

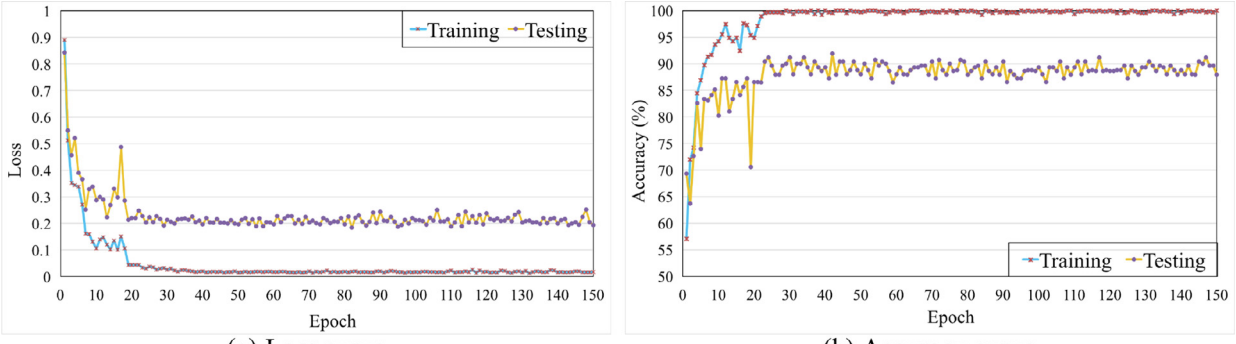

(a) Loss curve (b) Accuracy curve

Fig. 10. (a) The convergence curve of loss. (b) The convergence curve of accuracy.

Discussion

Altered connections in deep brain connectome

The core component of GBDM is the deep fusion of functional data and structural network: driven by the classification result, the graph that represents the learned connectome is iteratively updated based on functional features upon current network topology. Therefore, an interesting question would be how to understand and interpret the newly learned brain network – deep brain connectome. In the past decades, numerous connectome-based studies have reported and confirmed both structural and functional alterations in AD/MCI patients (Greicius et al. (2004); Wee et al. (2011); Agosta et al. (2012); Challis et al. (2015); Nir et al. (2015); Prasad et al. (2015); Chen et al. (2011, 2017); Yu et al. (2017)). However, the learned deep brain connectome cannot be treated as a simple combination of structural and functional connectivity. In this work, we conducted convolutional operations (see (8)) on graph-based neighbors which are defined by the adjacency matrix - $\hat{A}$. Essentially, the entry in $\hat{A}$ is proportional to the output at each layer and a larger connectivity in deep brain connectome indicates this connectivity may be potentially important in the classification task. In Table 2, most brain regions related to the increased connectivity are widely known for their close relations to AD/MCI development, such as orbital part of the inferior frontal gyrus (G_front_inf-Orbital) (Van Hoesen et al. (2000); Wang et al. (2007)) and temporal regions. This result suggests the training process of GBDM tends to alter brain network topology (initialized using structural network) to provide more efficient paths for convolution operations: by increasing or decreasing connectivity in current brain network ($\hat{A}$), the way of integrating information from neighbors can be optimized to improve the overall classification performance. In addition, it is not necessarily true that the structural and functional connectivity are always consistent as functional connectivity can be observed between brain regions with no direct connections (Damoiseaux & Greicius (2009); Honey et al. (2009); Park & Friston (2013)). Therefore, when incorporating functional data, the abovementioned training process will increase the connectivity between the regions in different hemispheres that have little or no structural connectivity (Fig. 5). Another interesting observation is the top increased connectivity inclines to connect brain areas with long distance, while decreased ones mostly connect local regions. In our graph convolutional operations, increasing/decreasing a connectivity will give more/less consideration to the related regions when combining functional features. Our results in Fig. 5 and Fig. 7 indicate the deep brain connectome tries to enhance the weight of long-distance connections instead of short-distance connections. Recent studies show that long-distance connections play a critical role in functional diversity and complexity of dynamics. Especially for AD and MCI, the severity of disease and cognitive impairment was more associated to long-distance connected regions (Liu et al. (2014); Cauda et al. (2020)). In general, the derived deep brain connectome reflects which connections/paths that are "important" to the classification task.

Strategies for overfitting in GBDM

Deep neural networks contain multiple non-linear hidden layers which makes them powerful when learning complicated relationships among data samples. However, with limited training data, it

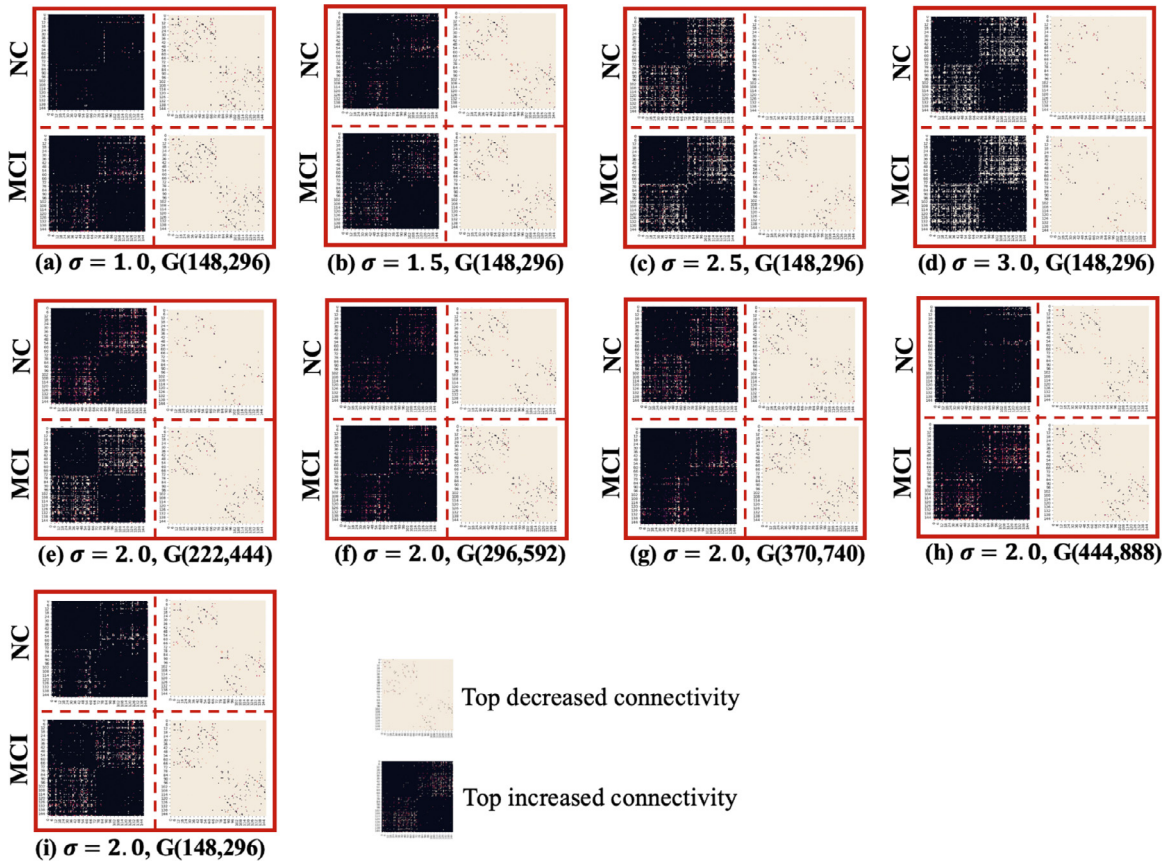

Fig. 11. Top increased and decreased connectivity under different model settings using the most recent released dataset (dataset-2) in ADNI. We used the same combinations of σ and feature dimension as Section 4.6 to conduct experiments on dataset-2. The complete comparison including structural network, deep brain connectome and the changed connectivity are shown in Fig. S3 and Fig. S4 in Supplementary.

is also possible to have overfitting issues. In deep learning field, several methods are proposed to solve the overfitting problem. A widely used strategy is data augmentation (Shorten & Khoshgoftaar (2019)) which aims to overcome the overfitting by artificially enlarging the training dataset. Because it may be difficult to directly evaluate the quality of the synthetic data, the improvement of the model performance (i.e. segmentation/classification accuracy) is the only criterion to justify the validity of the augmentation (Mok & Chung (2018); Hesse et al. (2020)). In this work, a major motivation is to study the fusion of brain structural and functional data and see how they affect each other when the fusion is driven by classification task. The augmented data may have unclear influence on the learned deep brain connectome even the overall classification accuracy improves, therefore, we do not adopt this strategy in our experiment. Our efforts for preventing overfitting focuses on model's architecture and the training process, such as batch normalization, early stop and dropout. Batch normalization (Ioffe & Szegedy (2015)) is a regularization that normalizes the set of activations in a layer by subtracting the batch mean from each activation and dividing by the batch standard deviation. Besides improving the speed of training process, it can make the learned model more stable and generalized. We performed batch normalization after each GCN layer. Early stopping (Caruana et al. (2001)) is a training strategy which can significantly reduce overfitting and improve the generalization of deep neural networks by terminating training at the point when performance on a validation dataset starts to degrade. We also adopted early stopping strategy in this work. Dropout (Srivastava et al. (2014)) is another widely used powerful method to address the overfitting problem. Previous study show that dropout can remarkably reduce overfitting and give major improvements over other regularization methods. In this work, we set 0.6 as the dropout ratio. We showed the curve of loss and accuracy of both training and testing dataset in Fig. 10. We can see that as the training progresses, the loss of testing dataset doesn't have obvious increase and the accuracy also converges smoothly.

Reproducibility and generalizability

Applying our method on large-scale multi-site imaging data is a good way to evaluate the robustness of our model. Here we used ADNI imaging dataset (one of the largest datasets of AD) which were collected from more than 60 centers. Besides the 214 subjects (from 32 centers) we used in Section 4, to better evaluate the reproducibility and generalizability of our model, we downloaded the most recent released subset of ADNI including 124 subjects (62NC (37 females, 25 males; 78.46 ± 8.67 yrs.) and 62MCI (35 females, 27 males; 77.96 ± 7.84 yrs.)) from other 28 centers as the second dataset (dataset-2). We applied the same data preprocessing, normalization steps and our method on this new dataset. We adopted 5-fold cross-validation to evaluate the same nine model settings as in Section 4.6. The classification performance and overall patterns of the changed connectivity are showed in Table 5 and Fig. 11. As shown in Table 5, the proposed model achieves similar classification performance – 94.1%. The pattern of changed connectivity showed in Fig. 11 is consistent with the patterns in Fig. 8. All these results indicate that our proposed model is stable and reproducible on different datasets.

The core idea of deep brain connectome is to identify the disease related brain network by learning the connectome topol-

Table 5
Classification Performance under Different Model Settings using Dataset-2.

Model Setting	Performance (%)						
Feature Dimension	σ	Acc[a]			Pre[b]	Rec[c]	Spec[d]
		Best	Worst	Ave[e]			
G(148, 296)	1.0	90.2	76.8	83.9	93.1	78.4	91.7
G(148, 296)	1.5	90.8	85.8	88.7	89.4	90.6	86.3
G(148, 296)	2.0	94.1	88.8	92.0	93.0	91.6	92.5
G(148, 296)	2.5	88.8	79.3	83.6	86.3	82.5	84.9
G(148, 296)	3.0	90.3	82.7	87.5	90.1	81.7	92.4
G(222, 444)	2.0	93.8	88.4	91.7	91.4	90.8	92.5
G(296, 592)	2.0	93.2	87.8	91.9	91.1	93.6	90.2
G(370, 740)	2.0	90.8	82.5	87.3	91.5	85.5	89.8
G(444, 888)	2.0	87.5	78.8	83.3	92.8	76.7	91.9

[a]Acc = Accuracy, [b]Pre = Precision, [c]Rec = Recall, [d]Spec = Specificity, [e]Ave = Average

ogy (using both structural and functional information) instead of fixing the predefined brain network. In this work, our proposed model has been applied to MCI/NC classification task, however, it can be easily extended to other tasks. In many brain disorders (Stam (2014); Fornito et al. (2015)), pathological changes tend to be "global" instead of "local": the structural and functional alterations are not equally distributed over the brain; instead, they often spread via structural or even functional network to influence other brain regions. Thus, our deep brain connectome can be a promising approach to explore the underlying relations between brain structural and functional perturbations at network level in both neurological and psychiatric diseases. In addition, by using appropriate label information including clinical status, subtyping or other cognitive/behavior measures, deep brain connectome can be used in the study of brain development, aging, disease progression and many other applications. For example, in section 3, classification loss is used to train the graph topology, but other loss options can be adopted based on different tasks, such as regression loss (e.g., for continuous measures) and task-specific loss (e.g., a combined loss for multiple tasks).

Conclusions

It is widely believed that the AD/MCI related brain alterations involve both brain structure and function. However, how to computationally model the complex and potentially non-linear relations between structural and functional data and integrate them at network level is still challenging. Inspired by the most recent development of deep learning approaches, in this work we developed a graph-based deep model – GBDM to classify MCI patients from normal controls. We constructed a graph convolutional network with trainable topology which is learned from functional features and structural network simultaneously. Comparing to the initialized structural network, the learned new brain network – deep brain connectome shows increased connections connecting to different hemispheres and regions with long-distance. Our developed GBDM achieves 92.7% classification accuracy on ADNI dataset and outperforms most recent studies. Given the complementary information stored in multimodal data, we envision that our proposed deep brain connectome can provide a promising way for the deep fusion of brain structure and function.

Declaration of Competing Interest

The authors declare that they have no known competing financial interests or personal relationships that could have appeared to influence the work reported in this paper.

Acknowledgements

This work is supported by STARTs from UT system. We thank the Alzheimer's Disease Neuroimaging Initiative (ADNI) database (adni.loni.usc.edu) for sharing valuable multi-modalities of brain imaging data.

Supplementary materials

Supplementary material associated with this article can be found, in the online version, at doi:10.1016/j.media.2021.102082.

References

Aderghal, K., Khvostikov, A., Krylov, A., Benois-Pineau, J., Afdel, K., Catheline, G., 2018. Classification of alzheimer disease on imaging modalities with deep cnns using cross-modal transfer learning. In: 2018 IEEE 31st International Symposium on Computer-Based Medical Systems (CBMS). IEEE, pp. 345–350.
ADNI: Alzheimer's disease neuroimaging initiative. http://adni.loni. usc.edu/.
Apostolova, L.G., Hwang, K.S., Kohannim, O., Avila, D., Elashoff, D., Jack Jr, C.R., Shaw, L., Trojanowski, J.Q., Weiner, M.W., Thompson, P.M., et al., 2014. Apoe4 effects on automated diagnostic classifiers for mild cognitive impairment and alzheimer's disease. NeuroImage: Clinical 4, 461–472.
Bullmore, E., Sporns, O., 2009. Complex brain networks: graph theoretical analysis of structural and functional systems. Nature reviews neuroscience 10, 186–198.
Caruana, R., Lawrence, S., Giles, C.L., 2001. Overfitting in neural nets: Backpropagation, conjugate gradient, and early stopping. In: Advances in neural information processing systems, pp. 402–408.
Cauda, F., Mancuso, L., Nani, A., Ficco, L., Premi, E., Manuello, J., Liloia, D., Gelmini, G., Duca, S., Costa, T., 2020. Hubs of long-distance co-alteration characterize brain pathology. Human brain mapping 41, 3878–3899.
Challis, E., Hurley, P., Serra, L., Bozzali, M., Oliver, S., Cercignani, M., 2015. Gaussian process classification of alzheimer's disease and mild cognitive impairment from resting-state fmri. NeuroImage 112, 232–243.
Chen, G., Zhang, H.-Y., Xie, C., Chen, G., Zhang, Z.-J., Teng, G.-J., Li, S.-J., 2013. Modular reorganization of brain resting state networks and its independent validation in alzheimer's disease patients. Frontiers in human neuroscience 7, 456.
Cheng, B., Liu, M., Zhang, D., Munsell, B.C., Shen, D., 2015. Domain transfer learning for mci conversion prediction. IEEE Transactions on Biomedical Engineering 62, 1805–1817.
Cui, Y., Wen, W., Lipnicki, D.M., Beg, M.F., Jin, J.S., Luo, S., Zhu, W., Kochan, N.A., Reppermund, S., Zhuang, L., et al., 2012. Automated detection of amnestic mild cognitive impairment in community-dwelling elderly adults: a combined spatial atrophy and white matter alteration approach. Neuroimage 59, 1209–1217.
Curran-Everett, D., 2018. Explorations in statistics: the log transformation. Advances in physiology education 42, 343–347.
Dai, Z., Lin, Q., Li, T., Wang, X., Yuan, H., Yu, X., He, Y., Wang, H., 2019. Disrupted structural and functional brain networks in alzheimer's disease. Neurobiology of Aging 75, 71–82.
Dai, Z., Yan, C., Wang, Z., Wang, J., Xia, M., Li, K., He, Y., 2012. Discriminative analysis of early alzheimer's disease using multi-modal imaging and multi-level characterization with multi-classifier (m3). Neuroimage 59, 2187–2195.
Daianu, M., Jahanshad, N., Nir, T.M., Toga, A.W., Jack Jr, C.R., Weiner, M.W., Thompson, P.M., 2013. Breakdown of brain connectivity between normal aging and alzheimer's disease: a structural k-core network analysis. Brain connectivity, 3, 407–422.
Damoiseaux, J.S., Greicius, M.D., 2009. Greater than the sum of its parts: a review of studies combining structural connectivity and resting-state functional connectivity. Brain Structure and Function 213, 525–533.
Daselaar, S.M., Iyengar, V., Davis, S.W., Eklund, K., Hayes, S.M., Cabeza, R.E., 2015. Less wiring, more firing: low-performing older adults compensate for impaired white matter with greater neural activity. Cerebral cortex 25, 983–990.
Destrieux, C., Fischl, B., Dale, A., Halgren, E., 2010. Automatic parcellation of human cortical gyri and sulci using standard anatomical nomenclature. Neuroimage 53, 1–15.
Dyrba, M., Grothe, M., Kirste, T., Teipel, S.J., 2015. Multimodal analysis of functional and structural disconnection in a lzheimer's disease using multiple kernel svm. Human brain mapping 36, 2118–2131.
Fan, Y., Resnick, S.M., Wu, X., Davatzikos, C., 2008. Structural and functional biomarkers of prodromal alzheimer's disease: a high-dimensional pattern classification study. Neuroimage 41, 277–285.
Fischl, B., 2012. Freesurfer. Neuroimage 62, 774–781.
Fling, B.W., Kwak, Y., Peltier, S.J., Seidler, R.D., 2012. Differential relationships between transcallosal structural and functional connectivity in young and older adults. Neurobiology of aging 33, 2521–2526.
Fornito, A., Zalesky, A., Breakspear, M., 2015. The connectomics of brain disorders. Nature Reviews Neuroscience 16, 159–172.
Franzmeier, N., Dyrba, M., 2017. Functional brain network architecture may route progression of alzheimer's disease pathology. Brain 140, 3077–3080.
Fries, P., 2005. A mechanism for cognitive dynamics: neuronal communication through neuronal coherence. Trends in cognitive sciences 9, 474–480.
Guo, J.L., Lee, V.M., 2014. Cell-to-cell transmission of pathogenic proteins in neurodegenerative diseases. Nature medicine 20, 130–138.

Hagmann, P., Sporns, O., Madan, N., Cammoun, L., Pienaar, R., Wedeen, V.J., Meuli, R., Thiran, J.-P., Grant, P., 2010. White matter maturation reshapes structural connectivity in the late developing human brain. Proceedings of the National Academy of Sciences 107, 19067–19072.
He, K., Zhang, X., Ren, S., Sun, J., 2016. Deep residual learning for image recognition. In: Proceedings of the IEEE conference on computer vision and pattern recognition, pp. 770–778.
Hesse, L.S., Kuling, G., Veta, M., Martel, A., 2020. Intensity augmentation to improve generalizability of breast segmentation across different mri scan protocols. IEEE Transactions on Biomedical Engineering.
Hinrichs, C., Singh, V., Xu, G., Johnson, S.C., Initiative, A.D.N., et al., 2011. Predictive markers for ad in a multi-modality framework: an analysis of mci progression in the adni population. Neuroimage 55, 574–589.
Hinton, G.E., Salakhutdinov, R.R., 2006. Reducing the dimensionality of data with neural networks. science 313, 504–507.
Hlinka, J., Paluš, M., Vejmelka, M., Mantini, D., Corbetta, M., 2011. Functional connectivity in resting-state fmri: is linear correlation sufficient? Neuroimage 54, 2218–2225.
Honey, C.J., Sporns, O., Cammoun, L., Gigandet, X., Thiran, J.-P., Meuli, R., Hagmann, P., 2009. Predicting human resting-state functional connectivity from structural connectivity. Proceedings of the National Academy of Sciences 106, 2035–2040.
Huang, Y., Xu, J., Zhou, Y., Tong, T., Zhuang, X., ADNI, A.D.N.I., et al., 2019. Diagnosis of alzheimer's disease via multi-modality 3d convolutional neural network. Frontiers in Neuroscience 13, 509.
Ioffe, S., Szegedy, C., 2015. Batch normalization: Accelerating deep network training by reducing internal covariate shift. arXiv preprint arXiv:1502.03167.
Jain, A., Nandakumar, K., Ross, A., 2005. Score normalization in multimodal biometric systems. Pattern recognition 38, 2270–2285.
Jenkinson, M., Beckmann, C.F., Behrens, T.E., Woolrich, M.W., Smith, S.M., 2012. Fsl. Neuroimage 62, 782–790.
Jie, B., Zhang, D., Gao, W., Wang, Q., Wee, C.-Y., Shen, D., 2013. Integration of network topological and connectivity properties for neuroimaging classification. IEEE transactions on biomedical engineering 61, 576–589.
Kazi, A., Shekarforoush, S., Krishna, S.A., Burwinkel, H., Vivar, G., Kortu m̈, K., Ahmadi, S.-A., Albarqouni, S., Navab, N., 2019. Inceptiongcn: receptive field aware graph convolutional network for disease prediction. In: International Conference on Information Processing in Medical Imaging. Springer, pp. 73–85.
Kipf, T.N., Welling, M., 2016. Semi-supervised classification with graph convolutional networks. arXiv preprint arXiv:1609.02907.
Ktena, S.I., Parisot, S., Ferrante, E., Rajchl, M., Lee, M., Glocker, B., Rueckert, D., 2018. Metric learning with spectral graph convolutions on brain connectivity networks. NeuroImage 169, 431–442.
LeCun, Y., Bengio, Y., Hinton, G., 2015. Deep learning. nature 521, 436–444.
LeCun, Y., Boser, B.E., Denker, J.S., Henderson, D., Howard, R.E., Hubbard, W.E., Jackel, L.D., 1990. Handwritten digit recognition with a backpropagation network. In: Advances in neural information processing systems, pp. 396–404.
Li, K., Guo, L., Zhu, D., Hu, X., Han, J., Liu, T., 2012. Individual functional roi optimization via maximization of group-wise consistency of structural and functional profiles. Neuroinformatics 10, 225–242.
Li, M., Qin, Y., Gao, F., Zhu, W., He, X., 2014. Discriminative analysis of multivariate features from structural mri and diffusion tensor images. Magnetic resonance imaging 32, 1043–1051.
Liu, F., Zhou, L., Shen, C., Yin, J., 2013. Multiple kernel learning in the primal for multimodal alzheimer's disease classification. IEEE journal of biomedical and health informatics 18, 984–990.
Liu, M., Cheng, D., Wang, K., Wang, Y., Initiative, ADNI, et al., 2018. Multi-modality cascaded convolutional neural networks for alzheimer's disease diagnosis. Neuroinformatics 16, 295–308.
Liu, M., Zhang, D., Adeli, E., Shen, D., 2015. Inherent structure-based multiview learning with multitemplate feature representation for alzheimer's disease diagnosis. IEEE Transactions on Biomedical Engineering 63, 1473–1482.
Liu, Y., Yu, C., Zhang, X., Liu, J., Duan, Y., Alexander-Bloch, A.F., Liu, B., Jiang, T., Bullmore, E., 2014. Impaired long distance functional connectivity and weighted network architecture in alzheimer's disease. Cerebral Cortex 24, 1422–1435.
Lynn, C.W., Bassett, D.S., 2019. The physics of brain network structure, function and control. Nature Reviews Physics 1, 318.
Meng, X., Jiang, R., Lin, D., Bustillo, J., Jones, T., Chen, J., Yu, Q., Du, Y., Zhang, Y., Jiang, T., et al., 2017. Predicting individualized clinical measures by a generalized prediction framework and multimodal fusion of mri data. Neuroimage 145, 218–229.
Min, R., Wu, G., Cheng, J., Wang, Q., Shen, D., Initiative, A.D.N, 2014. Multi-atlas based representations for alzheimer's disease diagnosis. Human brain mapping 35, 5052–5070.
Mok, T.C., Chung, A.C., 2018. Learning data augmentation for brain tumor segmentation with coarse-to-fine generative adversarial networks. In: International MICCAI Brainlesion Workshop. Springer, pp. 70–80.
Möller, C., Pijnenburg, Y.A., van der Flier, W.M., Versteeg, A., Tijms, B., de Munck, J.C., Hafkemeijer, A., Rombouts, S.A., van der Grond, J., van Swieten, J., et al., 2016. Alzheimer disease and behavioral variant frontotemporal dementia: automatic classification based on cortical atrophy for single-subject diagnosis. Radiology 279, 838–848.
Monti, F., Bronstein, M., Bresson, X., 2017. Geometric matrix completion with recurrent multi-graph neural networks. In: Advances in Neural Information Processing Systems, pp. 3697–3707.
Mori, S., Crain, B.J., Chacko, V.P., Van Zijl, P.C., 1999. Threedimensional tracking of axonal projections in the brain by magnetic resonance imaging. Annals of Neurology: Official Journal of the American Neurological Association and the Child Neurology Society 45, 265–269.
Parisot, S., Ktena, S.I., Ferrante, E., Lee, M., Guerrero, R., Glocker, B., Rueckert, D., 2018. Disease prediction using graph convolutional networks: application to autism spectrum disorder and alzheimer's disease. Medical image analysis 48, 117–130.
Park, H.-J., Friston, K., 2013. Structural and functional brain networks: from connections to cognition. Science 342.
Peng, J., Zhu, X., Wang, Y., An, L., Shen, D., 2019. Structured sparsity regularized multiple kernel learning for alzheimer's disease diagnosis. Pattern recognition 88, 370–382.
Petersen, S.E., Sporns, O., 2015. Brain networks and cognitive architectures. Neuron 88, 207–219.
Phillips, J.S., Da Re, F., Irwin, D.J., McMillan, C.T., Vaishnavi, S.N., Xie, S.X., Lee, E.B., Cook, P.A., Gee, J.C., Shaw, L.M., et al., 2019. Longitudinal progression of grey matter atrophy in non-amnestic alzheimer's disease. Brain 142, 1701–1722.
Plis, S.M., Amin, M.F., Chekroud, A., Hjelm, D., Damaraju, E., Lee, H.J., Bustillo, J.R., Cho, K., Pearlson, G.D., Calhoun, V.D., 2018. Reading the (functional) writing on the (structural) wall: multimodal fusion of brain structure and function via a deep neural network based translation approach reveals novel impairments in schizophrenia. Neuroimage 181, 734–747.
Roth, H.R., Lu, L., Liu, J., Yao, J., Seff, A., Cherry, K., Kim, L., Summers, R.M., 2015. Improving computer-aided detection using convolutional neural networks and random view aggregation. IEEE transactions on medical imaging 35, 1170–1181.
Schonberg, T., Pianka, P., Hendler, T., Pasternak, O., Assaf, Y., 2006. Characterization of displaced white matter by brain tumors using combined dti and fmri. Neuroimage 30, 1100–1111.
Schouten, T.M., Koini, M., De Vos, F., Seiler, S., Van Der Grond, J., Lechner, A., Hafkemeijer, A., Moller, C., Schmidt, R., De Rooij, M., et al., 2016. Combining anatomical, diffusion, and resting state functional magnetic resonance imaging for individual classification of mild and moderate alzheimer's disease. NeuroImage: Clinical 11, 46–51.
Shao, W., Peng, Y., Zu, C., Wang, M., Zhang, D., Initiative, A.D.N., et al., 2020. Hypergraph based multi-task feature selection for multimodal classification of alzheimer's disease. Computerized Medical Imaging and Graphics 80, 101663.
Shi, J., Zheng, X., Li, Y., Zhang, Q., Ying, S., 2017. Multimodal neuroimaging feature learning with multimodal stacked deep polynomial networks for diagnosis of alzheimer's disease. IEEE journal of biomedical and health informatics 22, 173–183.
Shorten, C., Khoshgoftaar, T.M., 2019. A survey on image data augmentation for deep learning. Journal of Big Data 6, 60.
Sirinukunwattana, K., Raza, S.E.A., Tsang, Y.-W., Snead, D.R., Cree, I.A., Rajpoot, N.M, 2016. Locality sensitive deep learning for detection and classification of nuclei in routine colon cancer histology images. IEEE transactions on medical imaging 35, 1196–1206.
Smith, S.M., Miller, K.L., Salimi-Khorshidi, G., Webster, M., Beckmann, C.F., Nichols, T.E., Ramsey, J.D., Woolrich, M.W., 2011. Network modelling methods for fmri. Neuroimage 54, 875–891.
Song, X., Zhou, F., Frangi, A.F., Cao, J., Xiao, X., Lei, Y., Wang, T., Lei, B., 2021. Graph convolution network with similarity awareness and adaptive calibration for disease-induced deterioration prediction. Medical Image Analysis 69, 101947.
Sporns, O., Chialvo, D.R., Kaiser, M., Hilgetag, C.C., 2004. Organization, development and function of complex brain networks. Trends in cognitive sciences 8, 418–425.
Srivastava, N., Hinton, G., Krizhevsky, A., Sutskever, I., Salakhutdinov, R., 2014. Dropout: a simple way to prevent neural networks from overfitting. The journal of machine learning research 15, 1929–1958.
Stam, C.J., 2014. Modern network science of neurological disorders. Nature Reviews Neuroscience 15, 683–695.
Sui, J., Adali, T., Yu, Q., Chen, J., Calhoun, V.D., 2012. A review of multivariate methods for multimodal fusion of brain imaging data. Journal of neuroscience methods 204, 68–81.
Sui, J., Huster, R., Yu, Q., Segall, J.M., Calhoun, V.D., 2014. Function-structure associations of the brain: evidence from multimodal connectivity and covariance studies. Neuroimage 102, 11–23.
Suk, H.-I., Lee, S.-W., Shen, D., Initiative, A.D.N., et al., 2014. Hierarchical feature representation and multimodal fusion with deep learning for ad/mci diagnosis. NeuroImage 101, 569–582.
Sun, L., Fan, Z., Ding, X., Huang, Y., Paisley, J., 2019. Region-of-interest undersampled mri reconstruction: A deep convolutional neural network approach. Magnetic resonance imaging 63, 185–192.
Supekar, K., Menon, V., Rubin, D., Musen, M., Greicius, M.D., 2008. Network analysis of intrinsic functional brain connectivity in alzheimer's disease. PLoS Comput Biol 4, e1000100.
Tang, X., Qin, Y., Wu, J., Zhang, M., Zhu, W., Miller, M.I., 2016. Shape and diffusion tensor imaging based integrative analysis of the hippocampus and the amygdala in alzheimer's disease. Magnetic resonance imaging 34, 1087–1099.
Tong, T., Gray, K., Gao, Q., Chen, L., Rueckert, D., Initiative, A.D.N., et al., 2017. Multi–modal classification of alzheimer's disease using nonlinear graph fusion. Pattern recognition 63, 171–181.
Tononi, G., Sporns, O., Edelman, G.M., 1994. A measure for brain complexity: relating functional segregation and integration in the nervous system. Proceedings of the National Academy of Sciences 91, 5033–5037.
Tsai, S.-Y., 2018. Reproducibility of structural brain connectivity and network metrics using probabilistic diffusion tractography. Scientific reports 8, 1–12.

Uludağ, K., Roebroeck, A., 2014. General overview on the merits of multimodal neuroimaging data fusion. Neuroimage 102, 3–10.
Van Hoesen, G.W., Parvizi, J., Chu, C.-C., 2000. Orbitofrontal cortex pathology in alzheimer's disease. Cerebral Cortex 10, 243–251.
Vemuri, P., Gunter, J.L., Senjem, M.L., Whitwell, J.L., Kantarci, K., Knopman, D.S., Boeve, B.F., Petersen, R.C., Jack Jr, C.R., 2008. Alzheimer's disease diagnosis in individual subjects using structural mr images: validation studies. Neuroimage 39, 1186–1197.
Vieira, S., Pinaya, W.H., Mechelli, A., 2017. Using deep learning to investigate the neuroimaging correlates of psychiatric and neurological disorders: Methods and applications. Neuroscience & Biobehavioral Reviews 74, 58–75.
Wang, K., Liang, M., Wang, L., Tian, L., Zhang, X., Li, K., Jiang, T., 2007. Altered functional connectivity in early alzheimer's disease: A resting-state fmri study. Human brain mapping 28, 967–978.
Wang, L., Gao, Y., Shi, F., Li, G., Gilmore, J.H., Lin, W., Shen, D., 2015. Links: Learning-based multi-source integration framework for segmentation of infant brain images. NeuroImage 108, 160–172.
Wang, L., Thompson, P.M., Zhu, D., 2019. Analyzing mild cognitive impairment progression via multi-view structural learning. In: International Conference on Information Processing in Medical Imaging. Springer, pp. 656–668.
Wee, C.-Y., Yap, P.-T., Zhang, D., Denny, K., Browndyke, J.N., Potter, G.G., Welsh-Bohmer, K.A., Wang, L., Shen, D., 2012. Identification of mci individuals using structural and functional connectivity networks. Neuroimage 59, 2045–2056.
Wu, Z., Pan, S., Chen, F., Long, G., Zhang, C., Philip, S.Y., 2020. A comprehensive survey on graph neural networks. IEEE Transactions on Neural Networks and Learning Systems.
Xie, T., He, Y., 2012. Mapping the alzheimer's brain with connectomics. Frontiers in psychiatry 2, 77.
Xing, E.P., Jordan, M.I., Russell, S.J., Ng, A.Y., 2003. Distance metric learning with application to clustering with side-information. In: Advances in neural information processing systems, pp. 521–528.
Ying, R., He, R., Chen, K., Eksombatchai, P., Hamilton, W.L., Leskovec, J., 2018. Graph convolutional neural networks for web-scale recommender systems. In: Proceedings of the 24th ACM SIGKDD International Conference on Knowledge Discovery & Data Mining, pp. 974–983.
Yu, G., Liu, Y., Shen, D., 2016. Graph-guided joint prediction of class label and clinical scores for the alzheimer's disease. Brain Structure and Function 221, 3787–3801.
Zhang, D., Shen, D., Initiative, A.D.N., et al., 2012. Multi-modal multi-task learning for joint prediction of multiple regression and classification variables in alzheimer's disease. NeuroImage 59, 895–907.
Zhang, D., Wang, Y., Zhou, L., Yuan, H., Shen, D., Initiative, A.D.N., et al., 2011. Multimodal classification of alzheimer's disease and mild cognitive impairment. Neuroimage 55, 856–867.
Zhang, L., Wang, L., Zhu, D., 2020a. Jointly analyzing alzheimer's disease related structure-function using deep cross-model attention network. In: 2020 IEEE 17th International Symposium on Biomedical Imaging (ISBI). IEEE, pp. 563–567.
Zhang, S., Dong, Q., Zhang, W., Huang, H., Zhu, D., Liu, T., 2019a. Discovering hierarchical common brain networks via multimodal deep belief network. Medical image analysis 54, 238–252.
Zhang, Y., Zhan, L., Cai, W., Thompson, P., Huang, H., 2019b. Integrating heterogeneous brain networks for predicting brain disease conditions. In: International Conference on Medical Image Computing and Computer-Assisted Intervention. Springer, pp. 214–222.
Zhang, Y.-D., Wang, S., Dong, Z., 2014. Classification of alzheimer disease based on structural magnetic resonance imaging by kernel support vector machine decision tree. Progress In Electromagnetics Research 144, 171–184.
Zhang, Z., Cui, P., Zhu, W., 2020b. Deep learning on graphs: A survey. IEEE Transactions on Knowledge and Data Engineering.
Zheng, W., Yao, Z., Li, Y., Hu, B., Wu, D., 2019. Brain connectivity based prediction of alzheimer's disease in patients with mild cognitive impairment based on multi-modal images. Frontiers in Human Neuroscience 13, 399.
Zhu, D., Li, K., Terry, D.P., Puente, A.N., Wang, L., Shen, D., Miller, L.S., Liu, T., 2014a. Connectome-scale assessments of structural and functional connectivity in mci. Human brain mapping 35, 2911–2923.
Zhu, D., Zhang, T., Jiang, X., Hu, X., Chen, H., Yang, N., Lv, J., Han, J., Guo, L., Liu, T., 2014b. Fusing dti and fmri data: a survey of methods and applications. NeuroImage 102, 184–191.